Published in final edited form as:
Nat Immunol. 2022 October ; 23(10): 1470–1483. doi:10.1038/s41590-022-01311-1.

Cellular and transcriptional dynamics of human neutrophils at steady state and upon stress

Elisa Montaldo[#1,14], **Eleonora Lusito**[#1], **Valentina Bianchessi**[#1], **Nicoletta Caronni**[#1], **Serena Scala**[1], **Luca Basso-Ricci**[1], **Carla Cantaffa**[1], **Alice Masserdotti**[1], **Mattia Barilaro**[1], **Simona Barresi**[1], **Marco Genua**[1], **Francesco Maria Vittoria**[1], **Giulia Barbiera**[1], **Dejan Lazarevic**[2], **Carlo Messina**[3], **Elisabetta Xue**[3], **Sarah Marktel**[3], **Cristina Tresoldi**[4], **Raffaella Milani**[5], **Paola Ronchi**[5], **Salvatore Gattillo**[5], **Luca Santoleri**[5], **Raffaella Di Micco**[1], **Andrea Ditadi**[1], **Giulio Belfiori**[6], **Francesca Aleotti**[6], **Matteo Maria Naldini**[1], **Bernhard Gentner**[1], **Elisa Gardiman**[7], **Nicola Tamassia**[7], **Marco Antonio Cassatella**[7], **Andrés Hidalgo**[8], **Immanuel Kwok**[9], **Lai Guan Ng**[9], **Stefano Crippa**[6,11], **Massimo Falconi**[6,11], **Francesca Pettinella**[7], **Patrizia Scapini**[7], **Luigi Naldini**[1,11], **Fabio Ciceri**[3,11], **Alessandro Aiuti**[1,11,12], **Renato Ostuni**[1,11,14]

[1]San Raffaele Telethon Institute for Gene Therapy (SR-Tiget), IRCCS San Raffaele Scientific Institute, Milan, Italy

[2]Center for Omics Sciences (COSR), IRCCS San Raffaele Scientific Institute, Milan, Italy

[3]Hematology and Bone Marrow Transplantation Unit, IRCCS San Raffaele Scientific Institute, Milan, Italy

[4]Molecular Hematology Unit, IRCCS San Raffaele Scientific Institute, Milan, Italy

[5]Immunohematology and Transfusion Medicine Unit, IRCCS San Raffaele Scientific Institute, Milan, Italy

[6]Pancreas Translational and Clinical Research Center, IRCCS San Raffaele Scientific Institute, Milan, Italy

[7]Section of General Pathology, Department of Medicine, University of Verona, Verona, Italy

[8]Area of Cell and Developmental Biology, Centro Nacional de Investigaciones Cardiovasculares Carlos III, Madrid, Spain

[14]Correspondence should be addressed to montaldo.elisa@hsr.it, ostuni.renato@hsr.it.

Author Contributions

E.M. and E.L. contributed to design the study, performed experiments, analyzed data, prepared figures, and edited the manuscript; E.M. performed immunophenotype analyses together with S.S. and L.B.R.; E.M., V.B., and N.C. generated transcriptome and functional data together with C.C., A.M., M.B., S.B., M.G., F.M.V., D.L., E.G., N.T., and F.P.; E.L. performed computational and statistical analyses, with some help from G.Ba.; C.M., E.X., S.M., C.T., R.M., P.R., S.G., L.S., G.Be., and F.A. selected and recruited study participants, collected biological samples, and acquired clinical information under the supervision of S.C., M.F., and F.C.; R.D.M., A.D., M.M.N., B.G., A.H., I.K., L.G.N, and L.N. provided key scientific inputs; M.A.C. and P.S. supervised E.G., N.T. and F.P., and contributed to data interpretation; A.A. supervised S.S. and L.B.R., and contributed to data interpretation; R.O. conceptualized and coordinated the study, acquired funding, analyzed the data, and wrote the paper. All authors read and edited the manuscript.

Competing Interests

The authors declare no competing interests

[9]Singapore Immunology Network (SIgN), A*STAR, Biopolis, Singapore

[11]Vita-Salute San Raffaele University, Milan, Italy

[12]Pediatric Immunohematology and Bone Marrow Transplantation Unit, IRCCS San Raffaele Scientific Institute, Milan, Italy

[#] These authors contributed equally to this work.

Abstract

Traditionally viewed as poorly plastic, neutrophils are now recognized as functionally diverse. However, the extent and determinants of neutrophil heterogeneity in humans remain unclear. We performed a comprehensive immunophenotypic and transcriptome analysis, at bulk and single-cell level, of neutrophils from healthy donors and patients undergoing stress myelopoiesis upon exposure to growth factors, transplantation of hematopoietic stem cells (HSC-T), development of pancreatic cancer, and viral infection. We uncover an extreme diversity of human neutrophils *in vivo*, reflecting the rates of cell mobilization, differentiation, and exposure to environmental signals. Integrated control of developmental and inducible transcriptional programs linked flexible granulopoietic outputs with elicitation of context-dependent functional responses. In this context, we detected an acute interferon (IFN) response in the blood of HSC-T patients that was mirrored by marked upregulation of IFN-stimulated genes in neutrophils but not in monocytes. Systematic characterization of human neutrophil plasticity may uncover clinically relevant biomarkers and support the development of diagnostic and therapeutic tools.

Neutrophils, the most abundant leukocytes in peripheral blood (PB), ensure host immunity by sensing and phagocytosing invading pathogens, as well as by releasing cytotoxic molecules via granule discharge or neutrophil extracellular traps (NETs)[1]. Individuals with severe congenital neutropenia or chronic granulomatous disease, diseases characterized by defective neutrophil development or functions, are indeed sensitive to opportunistic infections[2]; and rapid reconstitution of neutrophil counts after hematopoietic stem cell transplantation (HSC-T) is associated to higher survival and hematological recovery in chemotherapy-treated patients[3]. On the other hand, aberrant neutrophil activation underlies a variety of inflammatory conditions, including autoimmunity, stroke, neurodegeneration, and cancer[4].

The multifaceted activities of neutrophils in health and disease underscore a remarkable functional diversity[5]. In this context, traditional views of neutrophils as short-lived effectors with limited plasticity are challenged by findings that, already at the steady state, these cells persist within organs and acquire tissue-specific genomic programs[6]. Heterogeneity of neutrophils also reflects the output of bone marrow (BM) granulopoiesis, a demand-adapted process sensitive to homeostatic fluctuations[7], alterations of the hematopoietic niche, or changes in the concentration of mediators such as granulocyte-colony stimulating factor (G-CSF)[8]. During stress-induced myelopoiesis, committed precursors and immature neutrophils undergo expansion and premature release in the blood, where they co-exist with terminally differentiated subsets[9–11]. Neutrophil properties are further diversified as cells are exposed to stress-associated stimuli in the circulation or in target organs, leading to the production and release of a spectrum of inflammatory and regulatory products[12–16].

A systematic analysis of the phenotypic and transcriptome changes occurring in human neutrophils during inflammation is a prerequisite for the interpretation rational targeting of these cells' activities in homeostasis and disease. However, the extent and drivers of neutrophil heterogeneity in humans have remained elusive. We addressed these issues by performing a comprehensive immunophenotype and transcriptome analysis, at the bulk and single-cell level, of human neutrophils and monocytes in healthy controls and in patients undergoing stress-induced myelopoiesis driven by exposure to G-CSF, myeloablative conditioning followed by HSC-T, development of pancreatic ductal adenocarcinoma (PDAC), or infection with severe acute respiratory syndrome coronavirus 2 (SARS-CoV2).

Results

Dynamics and phenotype of G-CSF-elicited human neutrophils

To characterize stress-elicited neutrophil dynamics in humans, we performed a comprehensive immunophenotype analysis of PB or BM samples from control subjects and age-matched individuals undergoing G-CSF treatment (Supplementary Tables 1-6). On the one hand, unfractionated blood samples were analyzed using multiparametric flow cytometry with a panel of 16 antibodies able to quantify up to 28 subsets of hematopoietic stem and progenitor cells (HSPCs), committed precursors, and differentiated cells[17] (Extended Data Fig. 1a and Supplementary Table 7). To assess neutrophil phenotypes, PB and BM samples were additionally subjected to density gradient separation followed by targeted flow cytometry analyses of $CD15^+$ $CD66b^+$ cells that sedimented in the erythrocyte/granulocyte fraction (referred to as normal-density neutrophils, or NDNs) or in the mononuclear cell layer (low-density neutrophils, LDNs) (Extended Data Fig. 1b-d and Supplementary Table 7). Neutrophils indeed show variable buoyant densities according to changes in their granule content and nuclear morphology during maturation and/or activation. We observed a robust mobilization of myeloid-biased HSPCs in G-CSF-treated donors (Extended Data Fig. 1e-h), concomitant with a preferential surge of circulating neutrophils and other myeloid cells (Fig. 1a and Extended Data Fig. 1i,j). In line with previous studies[18,19], G-CSF exposure led to increased numbers of neutrophil precursors (SSC^{hi} CD33/$CD66b^+$ $CD38^+$ $CD11c^-$ $CD10^-$) and of immature neutrophils (SSC^{hi} CD33/$CD66b^+$ $CD38^-$ $CD11c^{-/+}$ $CD10^-$) (Fig. 1b,c and Extended Data Fig. 1a,k). G-CSF-treated donors displayed high frequencies of LDNs (Fig. 1d,e) that expressed low levels of the neutrophil differentiation and activation markers CD11b, CD11c, CD62L, CD16 and CD10 (Fig. 1d,f and Extended Data Fig. 2a). G-CSF-elicited LDNs were heterogeneous and included cells corresponding to neutrophil precursors ($CD15^+$ $CD66b^+$ $CD49d^+$ $CD16^-$), immature neutrophils ($CD15^+$ $CD66b^+$ $CD49d^-$ $CD16^{int}$), and mature neutrophils ($CD15^+$ $CD66b^+$ $CD49d^-$ $CD16^{hi}$) (Fig. 1g-i and Extended Data Fig. 2b,c)[9–11]. *Ex vivo* assays of 5-ethynyl-2'-deoxyuridine (EdU) incorporation confirmed that LDNs contained neutrophil precursors with proliferative potential[9,10] (Fig. 1j,k and Extended Data Fig. 2d,e). As reported previously[19], NDNs from G-CSF-treated donors were mostly composed of mature neutrophils with an activated phenotype – that is, lower expression of CD10 and CD62L (Fig. 1f and Extended Data Fig. 2a) and increased levels of CD35 (CR1) and CD54 (ICAM-1) (Extended Data Fig. 2f,g) than control NDNs. These data highlight the heterogeneous phenotype of G-CSF-elicited human neutrophils.

Dynamics and phenotype of neutrophils during HSC-T or PDAC

We next profiled neutrophil dynamics in age-matched subjects undergoing emergency myelopoiesis secondary to HSC-T with high-intensity conditioning (Supplementary Tables 1-6). PB and/or BM samples were collected from these patients shortly after treatment (1st follow-up, PB collected 16-27 days post HSC-T), at clinical recovery (2nd follow-up, PB and BM collected 28-40 days post-HSC-T), and months after HSC-T (3rd follow-up, PB and BM collected >180 days post-HSC-T) (Extended Data Fig. 2h-j). Flow cytometry analyses of unfractionated PB samples highlighted mobilization of phenotypically-defined neutrophil precursors in HSC-T patients at the first or second follow-up (Fig. 2a-c), coinciding with the appearance in the circulation of heterogeneous LDNs (Fig. 2d,e) containing proliferating and non-proliferating precursors as well as immature neutrophils (Fig. 2f,g and Extended Data Fig. 2d,e,k,l). We then analyzed PB samples from treatment-naïve patients with locally advanced or metastatic PDAC (n=19) or with intraductal papillary mucinous neoplasms (IPMN) (n=15), a type of lesion that often precedes tumor onset[20]. Total neutrophil counts were largely unaltered in PDAC patients, while those of other hematopoietic cells – HSPCs, monocytes and T lymphocytes – were significantly reduced (Extended Data Fig. 2m-p). Thus, the neutrophil-to-lymphocyte ratio (NLR), a frequently used marker of cancer progression[21], was higher for PDAC patients than for healthy controls or IPMN patients (Extended Data Fig. 2q,r). In line with previous reports[22], we observed increased frequencies of circulating LDNs in PDAC patients (Fig. 2h,i), with this cell population spanning cycling and non-cycling precursors, immature, as well as mature neutrophils (Fig. 2j and Extended Data Fig. 2s-v). We highlight that PDAC patients enrolled in the study are significantly older than healthy donors (Supplementary Tables 1, 3, 4). However, no increase in LDN frequencies nor NLR values were detected in age-matched IPMN patients (Fig. 2i and Extended Data Fig. 2r), suggesting that age is not a key determinant of neutrophil dynamics. Our results highlight mobilization of heterogeneous LDNs as a hallmark of stress myelopoiesis induced by G-CSF treatment, HSC-T, or PDAC.

Functional properties of G-CSF-elicited neutrophils

We next performed *ex vivo* experiments to assess reactive oxygen species (ROS) production, neutrophil extracellular trap (NET) release, and cytokine synthesis by neutrophil populations isolated from control or G-CSF-treated subjects (Fig. 3a). As compared to those of healthy individuals, NDNs from G-CSF-treated donors displayed a weaker respiratory burst upon treatment with phorbol myristate acetate (PMA) (Fig. 3b,c) – possibly reflecting the pre-activated phenotype of these cells *in vivo*. G-CSF-elicited LDNs also showed lower responses to PMA than controls (Fig. 3b,c), with ROS generation occurring mostly within phenotypically mature cells (Fig. 3d,e). Dose-response experiments revealed that, at a limiting dose of stimulus, LDNs from G-CSF-treated donors were substantially less able to produce ROS than matched NDNs (Fig. 3f). We also found that G-CSF-elicited LDNs underwent PMA-driven NETosis less efficiently than NDNs (Fig. 3g), corroborating the notion that LDNs contain neutrophils that have not fully acquired effector capacities. We next measured the levels of a panel of cytokines, chemokines, and growth factors in the culture supernatant of neutrophil populations treated *ex vivo* with the Toll-like receptors (TLR) 8 agonist resiquimod (R848), a powerful stimulator of cytokine release by human neutrophils[23]. A differential biosynthetic capacity emerged when comparing control and

G-CSF-elicited NDNs, with the latter cells displaying efficient release of inflammatory molecules upon stimulation (Fig. 3h). Notably, LDNs from G-CSF-treated donors were particularly responsive to TLR ligation and synthesized the highest levels of cytokines such as IL-1β, IL-1RA, G-CSF, CCL2, CCL5, and TNF-α (Fig. 3h). These findings suggest that, while lacking at least some effector features of terminally differentiated cells, mobilized immature neutrophils retain immune regulatory capacity via cytokine synthesis and release. Collectively, our data underscore the influence of maturation and exposure to growth factors on the functional effector and the immune regulatory properties of stress-elicited neutrophil subsets.

Bulk transcriptome analysis of monocytes, NDNs, and LDNs

To define the gene expression programs of myeloid cells at steady state and after stress, we performed bulk RNA sequencing (RNA-Seq) analyses of NDNs, LDNs, and monocytes isolated from the PB of healthy controls (n=19), of G-CSF-treated donors (n=17) as well as of HSC-T (n=8), PDAC (n=15) or IPMN (n=14) patients. We also analyzed neutrophil differentiation intermediates from BM samples of controls (n=3) or HSC-T patients (n=7), generating a total of 210 RNA-Seq samples from 73 individuals (Supplementary Table 8). Cell purity after magnetic bead selection or sorting was consistently higher than 95% (Extended Data Fig. 3a-f). Principal component analysis (PCA) and unsupervised k-means clustering highlighted clear segregation of monocyte, NDN, and LDN transcriptomes (Fig. 4a, Extended Data Fig. 4a-c and Supplementary Table 9). Monocytes were characterized by selective expression of transcripts encoding for known myeloid transcription factors (*KLF4, IRF8, MAFB*), scavenger receptors (*MARCO, MRC1*), components of the antigen presentation machinery (*HLA-DMA, HLA-DRA, CD74*) and inflammatory cytokines (*CCL2, CXCL10*) (Fig. 4a, module 6). Notably, monocytes expressed a gene program (module 5) that was shared with stress-elicited LDNs and that included transcripts encoding for regulators of RNA transcription (*POLR1A, POLR2L*), translation (*EIF2A, EEF2*) and ribosome biogenesis (*RPL10A, RPS23, BOP1*) (Fig. 4a). LDNs displayed high levels of genes encoding for neutrophil granule proteins (*MPO, DEFA4, ELANE*), cell cycle regulators (*TOP2A*), transcription factors (*CEBPE*), and surface markers (*CEACAM8*) (Fig. 4a, modules 2 and 4), and they tended to cluster together with developing neutrophils of the BM from healthy donors (Fig. 4a and Extended Data Fig. 4a-c). LDNs were also characterized by low basal expression of inflammatory response genes (*GBP1, OASL, IL1B, TNF*) that were instead transcribed in NDNs (Fig. 4a, modules 1 and 3) – a finding that was confirmed at the protein level for IL-1β (Extended Data Fig. 5a,b). Collectively, these data indicate that stress-elicited LDNs are characterized by a gene expression program distinct from that of monocytes or NDNs, and largely comparable to that of developing neutrophils of the BM.

Transcriptional responses to stress in NDNs and monocytes

We next set out to define stress-induced transcriptional changes in NDNs and monocytes (due to their heterogeneity, cells corresponding to LDNs were studied at the single-cell level, see below). Analysis of differentially expressed genes (DEGs) (Fig. 4b and Supplementary Tables 10-12) and downstream validation (Extended Data Fig. 5c-g) uncovered a profound transcriptome reprogramming of NDNs from G-CSF-treated donors or HSC-T patients,

while NDNs from PDAC patients underwent comparatively small changes. There was a limited overlap between DEGs in NDNs from the various experimental conditions, indicating that transcriptional responses of human neutrophils are largely stress-specific (Fig. 4c and Supplementary Table 13). In line with this notion, exposure to G-CSF led to induction in NDNs of genes belonging to gene ontology (GO) categories such as mitochondrial gene translation, oxidative phosphorylation, or leukocyte-mediated immunity, and to repression of interferon (IFN) responses (Fig. 4d and Supplementary Tables 14-16). On the other hand, NDNs from HSC-T patients showed a clear IFN signature, and they expressed genes of defense response and mitochondrial translation GOs (Fig. 4d and Supplementary Tables 14-16). Increased expression of IFN response genes and of transcripts controlling fatty acid metabolism was also measured in NDNs from PDAC patients (Fig. 4d and Supplementary Table 14-16). Notably, we found that monocytes from G-CSF-treated donors or HSC-T patients showed limited transcriptional changes as compared to what observed in NDNs from the same individuals (Fig. 4e, Supplementary Tables 17-22). These data highlight a remarkable plasticity of human neutrophils *in vivo*.

Analysis of plasma factors elicited by G-CSF, HSC-T or PDAC

To identify soluble factors underlying neutrophil dynamics upon stress, we quantified a panel of plasma cytokines, chemokines, and growth factors in the PB of subjects enrolled in the study (Supplementary Table 23). G-CSF administration was associated to a drastic up-regulation of G-CSF and IL-1RA, as well as to a mild increase of inflammatory cytokines that included IFN-γ, IL-18 and CXCL10 (Fig. 5a,b and Extended Data Fig. 6a). G-CSF treatment also led to lower levels of CXCL12 (Fig. 5a,b), a key BM homing signal for $CXCR4^+$ HSPCs and immature myeloid cells. We observed a marked inflammatory skewing of the plasma cytokine profile in HSC-T patients sampled up to one month after transplant, with increased levels of factors controlling myeloid cell differentiation (G-CSF, M-CSF, IL-6), recruitment (IL-8, CCL7, CCL3) and activation (IL-18, IL-12, IL-1a, IL-1β) (Fig. 5a,c). The most up-regulated plasma molecules in HSC-T patients were the IFN-stimulated chemokines CXCL9 and CXCL10, in line with a significant elevation of IFN-a2 and IFN-γ shortly after HSC-T (Fig. 5a,c). Patients with PDAC, but not with pre-malignant IPMN, also showed higher levels of pro-inflammatory cytokines, namely IL-6, IL-8, CCL3, and M-CSF as well as of CXCL9 and CXCL10 (Fig. 5a and Extended Data Fig. 6b). Our data indicate that G-CSF treatment, HSC-T or PDAC development are characterized by a systemic increase in PB concentration of inflammatory molecules known to drive stress myelopoiesis. In this context, plasma levels of G-CSF, IL-6 and IL-8 were positively associated with the frequencies of mobilized neutrophil precursors or LDNs when combining samples from all groups (Fig. 5d,e and Extended Data Fig. 6c-e). A correspondence between plasma cytokine profiles and transcriptional dynamics of neutrophils was evident, as exemplified by the increased levels of IFNs in PB and upregulation of IFN response genes in NDNs from HSC-T patients.

Transcriptional diversity of human neutrophils upon stress

We next performed single-cell RNA-Seq (scRNA-Seq) on $CD15^+$ cells isolated from PB or BM samples of healthy controls (PB n=2, BM n=2), G-CSF-treated donors (PB, n=4), HSC-T patients (PB n=3, of which one received G-CSF post-transplant, and BM n=2),

or PDAC patients (PB, n=5) (Supplementary Table 24). This sorting strategy enabled us to recover the full spectrum of developing neutrophils, from precursors to terminally differentiated cells (Extended Data Fig. 7a). After normalization and filtering, our dataset included transcriptomes from 130,628 cells, of which 1,059 were classified as contaminants (Supplementary Table 25). Graph-based clustering analysis revealed an extensive diversity of human neutrophils, with cells being distributed in the Uniform Manifold Approximation and Projection (UMAP) embedding according to their maturation stage, tissue location, exposure to stress signals and donor/patient identity (Fig. 6a,b, Extended Data Fig. 7b and Supplementary Table 25). We next employed curated gene signatures from developing human neutrophils[24,25] to annotate UMAP clusters (Fig. 6a-c and Extended Data Fig. 7c,d). Cells in cluster 1 expressed the highest levels of a transcriptional module previously associated to neutrophil-committed progenitors[25], which include genes encoding for azurophilic granules (*MPO, ELANE*) and cell cycle proteins (*MKI67, TOP2A);* we annotated this cluster as “precursors”. We then defined “early immature” (cl. 2, 3) and “immature” (cl. 4-14) neutrophils based on increasing expression of specific (*CAMP*, *LTF, LCN2*) or gelatinase (*MMP9, CTSB*) granule genes[24], which are progressively transcribed along the transitions from promyelocytes to band cells[25]. Finally, “mature” neutrophils (cl. 15-24) neutrophils were defined by expression of *SELL*, *MME*, and *CXCR4* in the BM or *NAMPT, CXCR2*, and *SOD2* in PB (Fig. 6a-c and Extended Data Fig. 7c,d). Mapping of neutrophil gene modules – previously defined by bulk RNA-Seq (Fig. 4a) – onto single-cell transcriptome data confirmed that LDNs (gene modules 2, 4 and 5) span precursors, early immature, immature, and mature neutrophils of the BM, while NDNs (module 1) correspond to mature PB neutrophils (Extended Data Fig. 7e). In line with the observed patterns of LDN mobilization, we found that scRNA-Seq clusters of precursors, early immature, and immature neutrophil were predominantly localized in the BM at steady state but became evident in the PB of G-CSF-treated donors, HSC-T or PDAC patients (Fig. 6a,b and Extended Data Fig. 7f,g). Neutrophils at various developmental stages showed differential patterns of inducible gene expression in response to stress. Mature cells from controls, G-CSF-treated donors, HSC-T or PDAC patients were segregated from each other in scRNA-Seq, while precursors and immature neutrophils from all experimental conditions tended to cluster together (Fig. 6a,b, Extended Data Fig. 7f,g and Supplementary Table 25). In this context, distinct gene signatures were evident in stress-elicited mature neutrophils. G-CSF exposure was associated to higher expression of transcripts such as *SERPINA1, CR1, CX3CR1, CD177, LAIR1*, and *CD14*, whereas neutrophils from a set of PDAC patients expressed IFN response genes (*IRF1, GBP1*) (Fig. 6a-c and Supplementary Table 26). Mature neutrophils from HSC-T patients sampled early after transplant expressed high levels of genes, such as *OAS2, CD274, AIM2, GBP5*) (Fig. 6a-c and Supplementary Table 26), that were associated to IFN responses (Fig. 6d). This signature became less evident at later time points (Fig. 6e,f and Supplementary Table 27), consistent with a progressive return to steady-state. Collectively, these data indicate that the combined mobilization and exposure to inflammatory factors drive divergent developmental trajectories in stress-elicited neutrophils, resulting in the acquisition of stimulus-specific gene expression programs (*e.g.*, IFN signature) in terminally differentiated cells (Extended Data Fig. 7h). More generally, our scRNA-Seq analyses uncover a high degree of transcriptional heterogeneity

of circulating human neutrophils, dictated by factors such as the differentiation state, their release in circulation, and the immunological status of the host.

Dynamics of neutrophil differentiation during stress

We next set out to dissect how exposure to stress signals impacted on the continuum of neutrophil differentiation. We first applied CellHarmony[26] on single-cell transcriptomes of PB and BM neutrophils from healthy controls to build a reference dataset of steady-state neutropoiesis, and to define cell states corresponding to specific developmental intermediates (Supplementary Table 28). Next, we matched scRNA-Seq data of neutrophils from PB and, when available, BM samples from G-CSF-treated donors, HSC-T and PDAC patients (termed query) to the previously defined CellHarmony clusters. This approach enables unbiased co-clustering of neutrophils at an equivalent maturation phase and precise quantification of stress-induced transcriptional changes (Fig. 7a,b, Extended Data Fig. 8a-c and Supplementary Tables 29-31). We observed clear differences in both the dynamics and the levels of expression of developmental genes in neutrophils from G-CSF-treated donors and HSC-T patients, with supra-physiological and prolonged expression of marker genes of neutrophil precursors (*MPO, DEFA4, ELANE, RNASE2, PLAC8*) (Fig. 7a-c, Extended Data Fig. 8c and Supplementary Tables 29, 30). Analogously, genes such as *TSPO, MMP8, HP, FCN1, FCER1G, S100A6* were hyper-expressed in immature neutrophils from G-CSF-treated donors and HSC-T patients, and they were prematurely and/or persistently transcribed even at earlier or subsequent differentiation stages (Fig. 7a-c, Extended Data Fig. 8c and Supplementary Tables 29-30). A similar, although less pronounced, behavior was observed in neutrophils from PDAC patients (Extended Data Fig. 8a,b and Supplementary Table 31). Our data show that exposure to inflammatory factors leads to substantial changes in the dynamics of expression of neutrophil developmental genes, possibly supporting the enhanced cellular outputs of granulopoiesis during stress.

Transcriptional changes of human neutrophils during stress

To determine how the pre-existing developmental state impacted on stimulus-induced reprogramming of neutrophils, we performed differential gene expression analyses between reference and query datasets in CellHarmony clusters. These studies uncovered sets of genes that were up- or down-regulated upon stress in a developmental state-specific manner (Fig. 7d,e, Extended Data Fig. 8d and Supplementary Tables 32-34). In HSC-T patients, transcripts up-regulated in differentiated neutrophils (such as *ISG15, IFI6* or *STAT1*) were poorly induced in precursors or in immature neutrophils (Fig. 7d,f and Supplementary Table 33). Conversely, genes induced in precursors were not induced in mature neutrophils (Fig. 7d,f and Supplementary Table 33). The latter behavior was also evident in cells from G-CSF-treated donors or PDAC patients, with stress-inducible gene expression programs being largely distinct between neutrophils at various developmental states (Fig. 7e,g and Supplementary Table 32). In line with this notion, gene ontologies of cluster-specific genes were distinct. Mature neutrophils from HSC-T patients up-regulated genes belonging to IFN response and antiviral defense GOs, while precursors and immature cells from the same individuals upregulated genes involved in RNA processing, translation, and protein biosynthesis (Fig. 7h and Supplementary Table 35). On the other hand, mature neutrophils from G-CSF-treated donors displayed high expression of genes related to ATP

and carbohydrate metabolic process, macrophage activation and cell adhesion (Fig. 7i and Supplementary Table 36). We observed a limited overlap between G-CSF-, HSC-T or PDAC-induced genes in CellHarmony clusters (Extended Data Fig. 8e and Supplementary Table 37), reinforcing the notion that transcriptional responses of neutrophil subsets are stress-specific. We next set out to validate and extend our findings in patients infected with severe acute respiratory syndrome coronavirus 2 (SARS-CoV2), an occurrence associated with emergency granulopoiesis and aberrant neutrophil activation[27,28]. Publicly available scRNA-Seq datasets of PBMCs from patients with coronavirus disease 19 (COVID-19)[27] were integrated with single-cell transcriptomes generated in this study and subjected to CellHarmony and differential gene expression analyses (Extended Data Fig. 9a). In keeping with our previous observations, viral infection altered both the dynamics and the expression levels of developmental genes in neutrophil mobilized upon stress (Extended Data Fig. 9b and Supplementary Table 38). Genes induced in neutrophils from COVID-19 patients differed for the various developmental intermediates (Extended Data Fig. 9c and Supplementary Table 39), and they were enriched in distinct GO categories (Extended Data Fig. 9d and Supplementary Table 40). Mature neutrophils from SARS-CoV2-infected individuals displayed an antiviral response signature that was absent or much less evident in precursors or immature neutrophils (Extended Data Fig. 9d). Indeed, differentiated neutrophils from COVID-19 patients – but not precursors or immature cells – up-regulated genes such as *IFITM3, LY6E, GBP1, GBP5, IFI6, ISG15*, and *FECR1G* (Extended Data Fig. 9e). Collectively, our data indicate that stress-elicited neutrophils undergo context-dependent transcriptome reprogramming *in vivo*, in a manner that reflects both the developmental stage and the type of stimuli to which the latter cells are exposed.

Transcriptional responses to IFN by developing neutrophils

Bulk and single-cell RNA-Seq analyses highlighted a marked tendency of differentiated human neutrophils to undergo transcriptome reprogramming in response to IFN. These cells showed dynamic expression of IFN-stimulated genes in HSC-T patients, to a degree that even surpassed that of monocytes from the same individuals (Fig. 4d,e and Supplementary Table 18). Furthermore, higher expression of IFN-stimulated genes was observed in mature neutrophils from HSC-T (or COVID-19) patients as compared to less differentiated cells (Fig. 7b,d,f and Extended Data Fig. 9b,c,e). To determine how the differentiation stage of neutrophils correlated with their transcriptional responses to IFNs, we performed scRNA-Seq on developing neutrophils treated *ex vivo* with IFN-β or IFN-γ. $CD15^+$ cells from CB samples of healthy donors were isolated and pooled to capture the entire spectrum of neutrophil maturation (Extended Data Fig. 10a-e and Supplementary Table 41). We obtained single-cell transcriptomes from 22,440 neutrophils, which clustered in the tSNE plot according to their developmental stage and the type of treatment (Fig. 8a-d, Extended Data Fig. 10e and Supplementary Table 42). The neutrophil composition of CB largely reflected that of BM and PB, with defined populations of precursors (cl. 1), immature (cl. 2) and mature neutrophils (cl. 3-6) (Fig. 8a,b and Extended Data Fig. 10e). Cluster 6 corresponded to a population of CB neutrophils expressing chemokine genes (*CXCL2*, *CCL3* and *CCL4*) that was not clearly detectable in BM or PB samples (Extended Data Fig. 10f) and was not investigated further. Treatment of mature neutrophils with IFN-β (cl. 4) or IFN-γ (cl. 5) led to up-regulation of antiviral response (*IFIT1, RSAD2, ISG15* and *OASL*)

or of known IFN-γ target genes (*GBP5, CD274, CD69* and *SOCS1*), respectively (Fig. 8e-g and Supplementary Table 43). On the other hand, precursors (cl. 1) or immature neutrophils (cl. 2) treated with IFNs did not segregate from controls in the scRNA-Seq analyses at the clustering resolution used (Fig. 8a-e and Supplementary Table 42). Developing neutrophils showed detectable but weaker induction of IFN-regulated genes than mature cells (Fig. 8f-i), suggesting lower responsiveness to cytokine stimulation. In line with this notion, *IFNAR1* and *IFNGR1* – transcripts encoding for key IFN-β and IFN-γ receptor subunits, respectively – were highly expressed in mature neutrophils, but not in immature neutrophils or in precursors (Fig. 8j,k). Collectively, our data underscore the extensive transcriptional plasticity of differentiated human neutrophils upon stimulation with environmental agents.

Discussion

In this study, we combined multiparametric immunophenotyping, quantification of plasma factors, bulk and single-cell genomics, and computational modeling to dissect cellular dynamics and molecular diversity of human neutrophils at homeostasis and upon stress. Our study extends previous analyses in mice[14,16,29–31], and it uncovers principles of neutrophil gene expression in relevant conditions of stress-induced myelopoiesis. Treatment with G-CSF of healthy subjects for HSC mobilization, HSC-T in chemotherapy-treated patients, and development of pancreatic cancer elicited a common immunological response, namely release in the blood of developing neutrophils and production of inflammatory cytokines driving neutrophil development and trafficking. The clinical outcomes of the above-described settings are profoundly influenced by neutrophil activities, as these cells were shown to control HSC mobilization in response to G-CSF or other agents such as GROβ and AMD3100[32], to enable immune protection of the host and vascular repair[33] upon HSC-T, and to modulate cancer progression in a context-dependent manner[4,34,35].

The properties of stress-elicited LDNs have been studied in various settings, often by bulk comparison with mature neutrophils[36]. We report that LDNs are highly heterogeneous and span the entire spectrum of neutrophil differentiation, up to early precursors. In keeping with their immature phenotype, LDNs displayed limited effector properties *ex vivo* – that is, respiratory burst and NETosis – as compared to terminally differentiated cells. On the other hand, LDNs were particularly efficient at producing cytokines upon TLR ligation, a capacity that was likely supported by the high expression level of transcript and protein biosynthesis genes. The functions of LDNs *in vivo* remain unclear and include immune modulation or tissue repair[37]. Our data support the hypothesis that LDNs regulate local and/or systemic inflammation via cytokine production. Furthermore, mobilized LDNs might give rise to mature neutrophils in periphery and thus support increased cellular demands upon inflammation or damage. In the context of HSC-T, mobilized neutrophil precursors may thus sustain immune reconstitution, and therapeutic approaches that stimulate their production and release could boost recovery from neutropenia following preparative conditioning. Combining lineage tracing with single-cell genomics and functional analyses will elucidate the hierarchy and developmental connections between neutrophil precursors and their progeny, as well as highlight functional implications during homeostasis and disease.

Single-cell transcriptome analysis of mobilized neutrophils exposed to inflammatory stimuli in the blood allowed us to dissect the complex interplay between differentiation and activation *in vivo*. Stress-elicited neutrophils underwent profound changes in the expression dynamics of developmental genes, and they concomitantly acquired stimulus-specific gene signatures. Notably, both the extent and the type of transcriptional responses to stimulation were different for cells at various maturation stages, with the most evident transcriptome dynamics being observed in differentiated neutrophils. These data support a model whereby combined mobilization and exposure to inflammatory factors elicit divergent neutrophil developmental trajectories that result in the acquisition of context-specific functional programs by terminally differentiated cells. We speculate that an integrated control of developmental and inducible gene expression in neutrophils enables persistent adaptations[38], such as those seen in long-term setting of trained immunity to infection or cancer[39,40].

Transcriptional reprogramming of neutrophils closely mirrored changes of blood cytokine profiles in subjects with stress myelopoiesis. A metabolic and proliferative response underlined neutrophils from G-CSF-treated donors, in line with the known biological actions of the latter molecule. An acute IFN cytokine signature was instead detected in the blood of HSC-T patients early after transplant, possibly reflecting chemotherapy-induced tissue damage, viral reactivation, exposure to pathogens, or acute graft versus host disease (GVHD)[41,42]; this response was associated with a marked induction of IFN-stimulated genes in circulating neutrophils. Strikingly, monocytes from the same HSC-T patients underwent minor transcriptional changes, as they upregulated a relatively small set of inflammatory genes. The molecular bases of differential IFN responses by neutrophils and monocytes *in vivo* remain to be elucidated. An intriguing possibility is that lower thresholds of IFN concentrations may be required to drive inducible gene expression in neutrophils; this behavior would be compatible with the existence of differential signal transduction pathways and chromatin dynamics at inflammatory response genes in the two cell types[43,44]. We propose that neutrophils act as powerful sensors of environmental stimuli - and of IFNs in particular - with the potential to provide accurate transcriptome readouts of signaling networks occurring in the blood. The high responsiveness of neutrophils to IFNs may underlie the relevance of these cells as biomarkers for severe infectious diseases, in line with the reported predictive power of neutrophil gene expression in blood transcriptional signatures of patients with bacterial or viral infection[45–47]. Future studies will be aimed at determining whether neutrophil transcriptome features can be used as biomarkers of clinical parameters of HSC-T, such as hematopoietic reconstitution, viral reactivation, infections with pathogens or GVHD.

By extending previous efforts to characterize neutrophil properties at the steady state[9,24,25] and in clinically relevant settings – including G-CSF administration[18], lung or heart disease[13,48], viral infection[27,28,49] and cancer[12,15,50], our study represents a step towards a mechanistic understanding of neutrophil diversity in humans. We anticipate that integration of current and future large-scale phenotypic, molecular, and functional analyses will enable the development of diagnostic and therapeutic strategies for diseases in which neutrophils are implicated.

Methods

Experimental Methods

Study participants and sample collection—Collection of biological samples was compliant to the Declaration of Helsinki and to the General Data Protection Regulation and it was approved by Ospedale San Raffaele and Azienda Ospedaliera Universitaria Integrata di Verona ethics committee (Protocols: TIGET09; MIELO-GEN; NEU-IPMN; CMRI/55742). A total of 149 participant were enrolled to the study between June 2017 and June 2022. Samples were collected into EDTA-containing sterile vacutainer tubes, stored at 25 °C, and processed within 2 hours. Informed consent was obtained by all participants. Participants received no compensation. Age and sex, as well as anonymized clinical information of enrolled participants are reported in Supplementary Tables 1-6.

Controls and G-CSF-treated donors: Healthy individuals were enrolled at Ospedale San Raffaele and Azienda Ospedaliera Universitaria Integrata di Verona. We collected peripheral blood (PB) from healthy donors before HSPC mobilization or bone marrow aspiration procedures (n=55). Bone marrow (BM) samples were harvested from the posterior iliac crests under anesthesia as standard HSPC donation procedure (n=14). Mobilized PB was collected from HSPC donors (n=49) after 5 days of treatment with G-CSF (Filgastrim, 10μg/kg per day). Cord blood (CB) samples (n=10) were collected after C-section deliveries at term of gestion of healthy volunteers donating placental tissue.

HSC-T patients: Patients (n=16) with hematological malignancies in complete remission were enrolled at Ospedale San Raffaele. They received preparative myeloablative conditioning and underwent post-transplant pharmacologic prophylaxis regimen to prevent acute and chronic Graft versus Host Disease (GvHD) and infections. Patients underwent allogeneic HSC-T from either haplotype-mismatched related donor (MMRD, n=12) or haplotype-matched related donor (MRD, n=4). 14 patients received unmanipulated G-CSF-mobilized PB cells, and 2 received unmanipulated BM cells. We collected samples at three time-points after HSC-T. 1st follow-up: early after transplant when white blood cell count reached 500 cells/μl for three days (PB collected 16-27 days post HSC-T); 2nd follow-up: at clinical recovery (PB and BM collected 28-40 days post-HSC-T); 3rd follow-up: long term after transplant (PB and BM collected >180 days post-HSC-T). Two patients (UPN34 and UPN40) showed delayed or absent engraftment after HSC-T. Among patients receiving post-transplant G-CSF, we only retained UPN47 for scRNAseq analysis.

PDAC and IPMN patients: We collected PB from patients with suspect or proven diagnosis of pre-malignant and malignant lesions of the pancreas at Ospedale San Raffaele. Intraductal papillary mucinous neoplasm (IPMN) diagnosis was confirmed by Magnetic Resonance Imaging (MRI) and/or cytological examination on specimens collected via Endoscopic Ultrasound Fine Needle Aspiration (EUS-FNA) or by histological examination after resection. Pancreatic ductal adenocarcinoma (PDAC) diagnosis was confirmed by cytological examination. Samples were retained only for patients with confirmed IPMN (n=15) or PDAC (n=19) diagnosis. Exclusion criteria were chemo- and/or radiotherapy

treatments and occurrence of acute pancreatitis, cholangitis and surgical or invasive endoscopic procedure within 1 month prior to PB collection.

Cell isolation—Mononuclear cells and granulocytes were separated by density centrifugation over a Lymphoprep (Stemcell technologies) gradient. PB and CB samples were diluted 1:1 with PBS, while BM and G-CSF-mobilized PB samples were diluted 1:4 with PBS and layered over Lymphoprep. Mononuclear cells were lysed with sterile ACK solution (0.15M NH_4Cl, 10mM $KHCO_3$, 0.1mM EDTA) 5 minutes at 25°C to remove residual erythrocytes and counted in the presence of Trypan blue (Sigma) to evaluate cell vitality. Monocytes and low-density neutrophils (LDN) were isolated from the mononuclear cell fraction either by FACS (see below) or by magnetic beads with CD14 Microbeads or CD15 Microbeads (Miltenyi Biotec), respectively. Granulocyte enriched fraction was further purified over Hetasep (Stemcell technologies) gradient followed by erythrocytes lysis and vital count with Trypan blue. Normal density neutrophils (NDN) were isolated from total granulocytes by magnetic bead sorting using the Neutrophil Isolation kit (Stemcell technologies). Alternatively, mononuclear cells and granulocytes were isolated by Ficoll-Paque (GE Healthcare Life Sciences) gradient centrifugation and Dextran (Sigma) gradient, as previously described[19]. For Cytochrome C reduction assay and supernatant production, total $CD66b^+$ neutrophils were isolated by magnetic bead selection by incubating mononuclear cells or granulocytes with fluorescence-conjugated anti-CD66b monoclonal antibody (mAb), followed by incubation with specific anti-fluorochrome microbeads (Miltenyi Biotec) according to the manufacturer's protocol. Purity of bead sorted cell subsets was evaluated by flow cytometry analysis. A detailed reagent list is reported in Supplementary Table 44.

Flow cytometry

Whole blood staining: Whole blood flow cytometry analysis was performed as described[17]. Briefly, 500 µl of PB or 100 µl of BM were incubated with 3ml or 1ml, respectively, of ACK solution for 10 minutes at 25 °C and washed twice with PBS. After a final wash in PBS 1% BSA, cells were resuspended in 100 µl of PBS 1% BSA and incubated with fluorochrome-conjugated antibody mix for 30 min at 25 °C in the dark. Cells were washed, resuspended in 100 µl of PBS 1% BSA and incubated 15 minutes in the dark with PI at a final concentration of 0.25 µg/ml. Samples were acquired at LSR-Fortessa or BD FACSymphony A5 SORP Cytometer (BD Biosciences) using DIVA software v8.0.2 (BD Biosciences). Data were analysed using Flowjo software v10.8.0 (Treestar). Cell populations were gated as previously described[17] with minor modification, as reported in Supplementary Table 7 and Extended Data Fig. 1a.

Mononuclear cells and granulocyte staining: Cells were resuspended in PBS containing 1% BSA or 2% FBS and 2 mM EDTA, and then incubated with FcR blocking reagent human (Miltenyi Biotec) or with 5% human serum at 25 °C for 5 minutes. Finally, cells were incubated with fluorochrome-conjugated antibody-mix for 20 minutes at 4°C in the dark. Cell suspension was washed with PBS 1% BSA and acquired at Navios Flow Cytometer using NAVIOS software v1.3 (Beckman Coulter), MACSQuant 10 or 16 Analyzers using MACSQuantify software v2.13 (Miltenyi Biotec). For IL-1β intracellular

staining, cells were fixed and permeabilized with IC Fixation Buffer (Thermo Fisher Scientific) and intracellular staining permeabilization buffer (BioLegend) according to manufacturer's instruction and acquired at or FACSCanto II using DIVA software v8.0.2 (BD Biosciences). Data were analyzed with FlowJo v10.6.2 (TreeStar)

Fluorescence activated cell sorting: PB monocytes, LDN and BM developmental intermediates were sorted from the mononuclear cell fraction. Samples were stained as described above and sorted at MoFlo XDP (Beckman Coulter) or FACSAria Fusion (BD Biosciences) cell sorters using Summit software v5.4 (Beckman Coulter) and DIVA software v8.0.2 (BD Biosciences), respectively. We sorted monocytes as $CD3^-CD56^-CD19^-CD34^-$ (Lin^-) $CD33^+$ $CD15^-$ $CD14^+$ cells and LDN as (Lin^-) $CD33^+$ $CD14^-$ $CD15^+$ $CD193^-$ cells. BM neutrophils were identified as (Lin^-) $CD14^-$ $CD33^+CD15^+$ $CD193^-$ cells and further fractionated into: BM1 $CD11b^-$ $CD16^-$ cells, BM2 $CD11b^+$ $CD16^-$ cells, BM3 $CD11b^+$ $CD16^{int}$, and BM 4 $CD11b^+$ $CD16^{hi}$ $CD10^+$ cells. For scRNAseq experiments, neutrophils were isolated from whole blood after lysis with RBC lysis buffer (BioLegend) and sorted as (Lin^-) $CD14^-$ $CD33^+$ $CD15^+$ cells. See also Supplementary Table 7. A detailed reagent list is reported in Supplementary Table 44.

EdU incorporation—Mononuclear cells or total granulocytes were plated at 10^6 cells/ml with RPMI + 10% FBS + 1% Gln + 1% Pen/strep in the absence or in the presence of 10 μM 5-ethylyn-2'deoxyuridine (EdU). After 18 hours of culture, cells were harvested, washed with PBS + 1% BSA, incubated with Fc blocking reagents (Miltenyi Biotec) and stained. Cells were fixed, permeabilized and incubated with reaction cocktail according to Click-iT Plus EdU FlowCytometry Assay kit (Thermo Fisher Scientific). Samples were acquired at Navios Flow Cytometer using NAVIOS software v1.3 (Beckman Coulter) and analyzed with FlowJo v10.6.2 (TreeStar). A detailed reagent list is reported in Supplementary Table 44.

ROS production—Cytochrome C reduction assays or Neutrophil/monocyte respiratory burst assay kits (Cayman chemical) were used. Freshly isolated $CD66b^+$ LDNs and/or NDNs were washed and resuspended at $2x10^6$ cells/ml in Hank's Balanced Salt Solution (HBSS) pH 7.4, supplemented with 10 % FBS, 0.5 mM CaCl2 and 1 mg/ml glucose. O_2^- production in response to 20 ng/ml PMA (Sigma) was assessed by the Cytochrome C reduction assay (Cayman), as previously described[51]. For flow cytometry analysis of ROS, $1x10^5$ mononuclear cells or granulocytes were incubated with Dihydrorhodamine-123 (Cayman chemical) and left untreated or stimulated with PMA 20 ng/ml for 15 or 30 minutes. Cells were stained with fluorochrome-conjugated antibodies as described above, acquired at FACSCanto II using DIVA software v8.0.2 (BD Biosciences) and analyzed with FlowJo v10.6.2 (TreeStar). LDNs and NDNs were identified after gating on Lin^- $CD15^+$ cells in the PBMC and granulocyte fraction, respectively. A detailed reagent list is reported in Supplementary Table 44.

NETosis—The NETosis assay kit (Cayman) was used. Bead-sorted NDNs and LDNs were resuspended at $1x10^6$ cells/ml and left untreated or stimulated with PMA 20nM and incubated at 37°C for 2 hours. Culture supernatants were removed, and wells were washed to remove soluble elastase. After treatment with S7 nuclease to induce the

release of NET-associated elastase, supernatants were collected, and elastase activity was evaluated according to manufacturer's instructions. A detailed reagent list is reported in Supplementary Table 44.

***Ex vivo* stimulation of NDNs and LDNs—**Purified LDNs and NDNs were plated at $5x10^6$/ml in the presence of RPMI 1640 medium supplemented with 10% FBS and treated or not with 5 μM R848 (InvivoGen). After 20 hours of culture at neutrophils were collected and spun at 300 x g for 5 minutes. Cell-free supernatants were immediately frozen and stored at -80°C until use. A detailed reagent list is reported in Supplementary Table 44.

Plasma collection—An aliquot of 300μl of blood collected into EDTA tubes was centrifuged 5 minutes at 10,000 x g. Plasma was transferred into a clean tube and re-centrifuged 5 minutes at 10,000 x g. Plasma was frozen and stored at -20°C until use.

ELISA—Cytokine and chemokine concentration in culture supernatants or plasma were measured using Bio-Plex Pro Human Cytokine Screening Panel, 48-Plex (Biorad) according to the manufacturer's instructions. Acquisition was performed using Luminex instruments and analyzed with Bio-plex manager (Biorad) software. A detailed reagent list is reported in Supplementary Table 44.

Cytospin and May-Grünwald Giemsa staining—We resuspended 100,000 cells in 200 ml of PBS + 2% FBS and deposited on a slide with a Cytospin 4 centrifuge (Thermo Fisher Scientific). Slides were dried 30 minutes at 25 °C and stained with May-Grünwald solution (Carlo Erba) for 5 min. After washing with water, slides were stained with Giemsa (Merck) working solution (Giemsa solution diluted 1:10) for 15 min and washed with water. Slides were dried in upright position at 25 °C. Images were acquired in bright field using an Eclipse (Nikon) microscope and NIS-Elements 4.0 software. A detailed reagent list is reported in Supplementary Table 44.

Real-Time quantitative PCR—RNA was extracted using the ReliaPrep RNA Cell Miniprep System (Promega) and measured with Qubit RNA HS Assay Kit using a Qubit 3.0. 0.5 ng of RNA were retrotranscribed with SuperScript II, and cDNA was PCR-amplified with KAPA HiFi HotStart. Target genes amplification was done with Fast SYBR Green Master Mix on a ViiA 7 Real-Time PCR System. A detailed reagent list is reported in Supplementary Table 44.

***Ex vivo* stimulation of CB neutrophils—**We isolated mononuclear cells and granulocytes, as reported above, from three different CB samples. From the mononuclear cell fraction, we isolated LDNs by performing a double round of magnetic bead sorting using Neutrophil Isolation kit (Stemcell technologies). From the granulocyte cell fraction, we isolated NDNs by performing a single round of magnetic bead sorting using Neutrophil Isolation kit (Stemcell technologies). To ensure a sufficient representation of neutrophil precursors (less abundant cell population) and of NDNs (less efficiently detected by droplet-based scRNA-Seq due to loe RNA content), LDNs and NDNs from each CB sample were mixed in a ratio of 1:3. We plated LDN-NDN mix at 10^6 cells/ml in RPMI 1640 + 10% FBS + 1% Gln + 1% Pen/strep alone or with G-CSF, IFN-β or IFN-g all used at 10ng/ml.

Europe PMC Funders Author Manuscripts

After 4h, cells were harvested, washed, counted and for each condition we mixed cells from different CB in a ratio 1:1:1. The pooled samples were processed for scRNAseq as described below. A detailed reagent list is reported in Supplementary Table 44.

Bulk RNA sequencing—We extracted total RNA using the ReliaPrep RNA Cell Miniprep System (Promega). RNA concentration was measured with Qubit RNA HS Assay Kit using Qubit 3.0 and RNA integrity was evaluated with Agilent RNA 6000 Pico Kit using Bionalyzer (Agilent). RNA-Seq libraries were generated using the Smart-seq2 method[52] starting from 0.5 ng of RNA. Retro-transcription was performed using SuperScript II Reverse Transcriptase, cDNA was PCR-amplified (18 cycles) with KAPA HiFi HotStart and purified with AMPure XP beads. After purification, we determined cDNA concentration using Qubit dsDNA HS Assay Kit at Qubit 3.0 and we assessed size distribution at Agilent 4200 TapeStation system. We performed the tagmentation reaction starting from 0.5 ng of cDNA for 30 minutes at 55°C and we performed enrichment PCR using 12 cycles. Libraries were purified with AMPure XP beads, quantified using Qubit 3.0, assessed for fragment size distribution on an Agilent 4200 TapeStation system. Libraries were sequenced on an Illumina Next-Seq500 or NovaSeq6000 (single-end, 75bp read length) according to the manufacturer's instruction. A detailed reagent list is reported in Supplementary Table 44.

Single-cell RNA sequencing—We isolated total $CD15^+$ cells and LDN (from one G-CSF stimulated donor) by cell sorting. We generated scRNA-Seq libraries using the microfluidics-based approach of Chromium Single-Cell Controller (10X Genomics) using the Chromium Single Cell 3' Reagent Kit v3.0 according to the manufacturers' instructions. In each experiment we loaded sample in order to obtain a target cell recovery of 10,000 cells. cDNA amplification was performed using 13 PCR cycles. The concentration of the scRNA-seq libraries was determined using Qubit dsDNA HS Assay Kit at Qubit 3.0 and size distribution was assessed using an Agilent 4200 TapeStation system. Libraries were sequenced on an Illumina NextSeq500 or NovaSeq6000 instruments (paired-end, 150bp read length) according to the manufacturer's instruction. A detailed reagent list is reported in Supplementary Table 44.

Computational methods

Bulk RNA-Seq analyses on NDNs, LDNs, and monocytes

Data processing: Single-end reads (75 bp) were mapped to the GRCh38 reference genome using STAR aligner (v.2.6.0a)[53]. The FeatureCounts function from Rsubread package (v.3.7)[54] was then used to summarize the aligned reads to NCBI *Homo sapiens* RefSeq genes (hg38) while setting the minMQS option to 3. Downstream analyses on the count matrix of expressed genes (25,064 genes and 210 samples) were performed in R environment (v 4.0.1) with edgeR R package (v. 3.20.7)[55]. First, genes with more than one count-per-million (cpm) in at least 15% of the total set of samples (NDNs, LDNs and monocytes) were retained for a total of 8,419 genes and 210 samples. Read counts of expressed genes were then normalized with the Trimmed Mean of M-values (TMM) method[56] using calcNormFactors function. The weighted likelihood empirical Bayes method[57,58] was used to calculate the posterior dispersion estimates through the estimateDisp function. The ComBat_seq function[59] from the sva package (v. 3.38.0)[60] was

used to model and correct the batch effects between the sequencing runs. The principal component analysis (PCA) of the samples was performed based on the batch-corrected reads per count million.

Heatmap of variable genes: Log2 (cpm +1) were calculated from the batch corrected counts and used to compute the gene-wise variance across all samples. The values above the 80th percentile of the resulting variance distribution were selected, and the corresponding genes used to perform the unsupervised *k*-means cluster analysis on the standardized expression values with *k* equal to six. Hierarchical cluster analysis (HCL) was then performed on the gene modules and samples using the Pearson correlation as distance method and the ward.D2 agglomerative algorithm as hierarchical clustering method.

Differential gene expression analysis: Low density neutrophils (82 samples) were removed from the raw count matrix generated with the FeatureCounts R function. The resulting matrix was composed by 25,064 genes and 128 samples: 70 NDNs and 58 monocytes. Genes with more than one cpm in at least 15% of the NDNs or monocytes were selected. The resulting matrix was composed by 8,362 genes and 128 samples. Read counts were normalized and corrected for batch effects as above. Differential gene expression analysis of myeloid cells after stress with respect to the steady state was performed with edgeR for NDNs and monocytes independently starting from the adjusted count matrix containing both cell types. NDNs and monocytes were selected and the two datasets were further divided into three stress-related/steady state datasets, each composed by samples from one of the stress condition (G-CSF, HSC-T and PDAC) and samples at steady state. Only genes with cpm >1 in at least 30% of the samples composing each sub-dataset were retained. The differential gene expression analysis for each stress and cell type was performed by fitting a negative binomial generalized linear model with robust hyperparameter estimation[57,61] using the glmQLFit function and after computing the dispersion with estimateDisp function. A quasi-likelihood (QL) F-test[62,63] was then performed using the glmQLFTest function. The sequencing run ID was included in the design matrix of each comparison as covariate. Genes with abs(Log2FC) >=1.5 and FDR < 0.05 were considered to be differentially expressed.

Principal Component Analysis: Principal Component Analysis of NDN, LDN and Monocytes was performed on expressed genes with cpm > 1 in at least 30% of the total samples of each cell type and with a variance greater than the 95th percentile of the distribution of gene-wise computed variances.

Gene Set Enrichment Analyses: For each stress condition and cell type, differentially expressed genes were ranked by decreasing order of log2FC in stress versus steady-state. GSEA (v. 4.0.3)[64] was performed on ranked gene lists using GO Biological Process ontology (c5.go.bp.v.7.4) as Gene Sets, with number of permutations equal to 1,000.

Single-cell RNA-Seq analyses of PB and BM neutrophils

Data processing: Fastq files were generated from raw Illumina BCL files using Cell Ranger v6.0.2 (10X Genomics) with cellranger mkfastq and default parameters. Cell Ranger count was then used to align sequencing reads to the reference transcriptome GRCh38, to perform

UMI filtering and barcode and UMI counting. Only confidently mapped reads with valid barcodes, unique molecular identifiers (UMIs) and non-PCR duplicated were retained by the tool. The overall sequencing quality was evaluated by looking at the summary metrics of the web_summary.html file generated by the cellranger pipeline for each sample. The Seurat v4.0.5 R package (https://satijalab.org/seurat/) was then used to perform all downstream analysis. First, we removed cells expressing less than 300 unique genes and genes expressed in less than 3 cells from the non-normalized UMI count matrix of each sample. Raw count matrices of all samples were then combined in a single Seurat object (17,625 genes and 143,485 cells) with the use of the merge function. A cell/gene quality control was then performed. We jointly examined the distribution of the count depth (i.e. the number of counts per barcode), of the number of genes per barcode and of the fraction of counts from mitochondrial genes per barcode. Outlier peaks were then filtered out by thresholding. Cells with a total number of detected molecules < 500 indicating low quality cells or empty droplets were discarded. We also removed cells with a percentage of reads that map to the mitochondrial genes greater than 10% and cells with a number of detected genes > 4,000. The two filters were respectively used to remove low-quality/dying cells and cell doublets or multiplets with an aberrantly high gene count[65]. We also applied a gene-wise filter on the average counts to remove low-abundance genes[62]. The filter threshold was established looking at the distribution of the average counts. Genes with a value less than the 15th percentile of the distribution were removed. The final raw count matrix was composed by 15,020 genes and 130,628 cells. We then applied the sctransform normalization[66] (SCTransform function) while adjusting for the following confounding sources of variation: the mitochondrial mapping percentage and the cell cycle scores computed with the CellCycleScoring function. Data were then scaled with ScaleData and the top 1,000 variable features were selected with the “vst” method of the FindVariableFeatures function. Shared Nearest Neighbor (SNN) graph was constructed using the FindNeighbors function taking as input the first 50 principal components, computed with RunPCA function. Cell clusters were defined using a resolution of 1.5, calculated with the FindCluster function and were visualized in two dimensions using uniform manifold approximation and projection (UMAP)[67]. Cluster-specific marker genes were identified using MAST method[68] through the FindMarkers function with option only.pos = TRUE, min.pct = 0.1 and setting a cut-off of FDR < 0.05.

The scRNA-seq data of patients with COVID-19 generated by Schulte-Schrepping[27] were downloaded from FASTGenomics database at https://beta.fastgenomics.org/datasets/detail-dataset-7656cfe94fb14a01b787f4774e555036. The dataset used in our analysis was PBMC 10x from cohort2 (Bonn cohort) composed by 46,611 genes and 3,154 cells relative to 22 COVID-19 patients. From the pre-analyzed seurat_COVID19_Neutrophils_cohort1_10x_jonas_FG_2020-08-19.rds file, we extracted the raw counts and re-analyzed the data by applying the quality control criteria used for our datasets to ensure the methodological consistency however conditioned to the distribution and features of the data. We first removed the cells expressing less than 300 unique genes and genes expressed in less than 3 cells from the non-normalized UMI count matrix resulting in 13,957 genes across 3,138 cells. Based on the visual inspection of the distribution of the detected molecules across the retained cells, we removed cells with

less than 500 detected transcripts indicating low quality cells or empty droplets. We also removed cells with more than 10% mitochondrial reads, and with > 2,000 detected genes indicating putative doublets or multiplets. Genes with few counts (i.e. less than the 15th percentile based on the distribution of the average gene-wise counts across all cells) were considered uninformative and removed. According to the applied criteria for the quality control of cells and genes, the dataset was finally composed by 12,113 genes and 2,990 cells. On this data we performed the normalization, the identification of the highly variable features, the scaling, the linear dimensionality reduction, and the clustering as described above. A batch-effect correction on the normalized expression matrix was performed to run cellHarmony, using ComBat from the sva package to adjust for potential batch effects between donors.

Gene Set Enrichment Analysis: Top 50 marker genes were ranked by decreasing order of log2FC > 0. GSEA (v. 4.0.3)[64] was performed on ranked gene lists using GO Biological Process ontology (c5.go.bp.v.7.4) as Gene Sets, with number of permutations equal to 1,000.

Cell Harmony analyses: scRNA-seq raw count matrices of G-CSF-treated donors, HSC-T patients, PDAC patients and PB or BM healthy (HD) donors were merged for each condition and preprocessed and normalized with Seurat v4.0.5 using the same criteria and methods as described above with the following exceptions: cells with a percent of mitochondrial genes greater than 25%, 10%, 15% and 10% relative to G-CSF, HSC-T, PDAC and HD respectively, were removed. The threshold for putative doublets and multiplets was also changed and established to be 3,500 for G-CSF and 4,500 for PDAC after the joint visualization of the number of genes and counts. It remained unchanged for HSC-T and HD datasets. A batch-effect correction was additionally applied to the normalized count matrix of each dataset using ComBat[69,70] from the sva package (v3.38.0) to adjust for potential batch effects between donors of the same condition. CellHarmony[26] was then applied to match cells at the same differentiation stage between the healthy condition (the reference) and the stress (the query). First, the reference dataset (15,851 HD cells: 10,173 BM cells and 5,678 PB cells) was subjected to an unsupervised analysis with ICGS v2 (AltAnalyze version 2.1.2) that identified 8 distinct clusters corresponding to discrete differentiation stages of bone marrow and blood neutrophils. Two of them were considered contaminants and removed. Options were accepted by default except for the number of ICGS cluster (k) that was set to 15 and the column clustering method that was “hopach”. Cells from each stress condition (G-CSF: 30,787 cells, HSC-T: 39,479 cells, PDAC: 21,153 cells, COVID-19: 2,990 cells) were then matched to the reference with cellHarmony to identify analogous differentiation stages. Pairwise differential gene expression analysis between the query cells and the reference cells was performed for each cluster and for each stress independently with FindMarkers function of Seurat v4.0.5 R package using MAST method on jointly preprocessed and SCT-normalized expression matrices (i.e. Steady state + G-CSF; Steady state + HSC-T; Steady state + PDAC; Steady state + COVID-19). The minimum detection rate (min.pct) was set to 20%. Genes with Log2FC >=1 and FDR < 0.05 were further considered to be differentially expressed.

Gene Set Enrichment Analysis: Due to the small gene set size of the gene lists generated by applying the Log2FC >=1 threshold, the full-length gene lists previously identified with FindMarkers by applying only the detection rate cut-off of 20% were used to run the GSEA. Genes were ranked by decreasing order of log2FC in stress versus healthy for each cluster of differentiation. The gene set enrichment analysis was performed on ranked gene lists using GO Biological Process ontology (c5.go.bp.v.7.4) as Gene Sets, with number of permutations equal to 1,000.

Single-cell RNA-Seq analyses of CB neutrophils—Chromium single-cell RNA-seq raw data were preprocessed with Cell Ranger v6.0.2 (10X Genomics) as described above. Filtered UMI count matrices of CB neutrophils unstimulated (control), stimulated with IFN-β, IFN-γ and G-CSF were analyzed with Seurat v4.0.5 R package. Data were first subjected to quality control and cells and genes were selected/removed based on the same criteria described above (i.e. min.cells = 3, min.features = 300, percent.MT < 10; nFeature_RNA < 4,000; nCount_RNA > 500). The 20^{th} percentile of the overall distribution of gene expression levels was used as threshold to remove poorly expressed genes. Data (13,813 genes and 22,440 cells) were then SCT-normalized and scaled while adjusting for cell-cycle effects and the mitochondrial percentage. Top 1,000 variable features were selected with the “vst” method and used as input for the principal component analysis. Shared Nearest Neighbor (SNN) graph was constructed using the FindNeighbors function taking as input the first 50 principal components, computed with RunPCA function. Cell clusters were defined using a resolution of 0.3, calculated with the FindCluster function and were visualized in two dimensions using the t-distributed stochastic neighbor embedding (t-SNE). Cluster-specific marker genes were identified using MAST method through the FindMarkers function. Only genes expressed in at least 10% of either of the two groups were tested.

Statistics and Reproducibility—No statistical method was used to predetermine sample size. No data were excluded from the analysis. Datasets used for the specific analyses are reported in the Methods section. Statistical assumptions – including data distribution, independence of observations and homogeneity of variance – were considered for each dataset, and statistical tests were performed accordingly. The experiments were not randomized. The investigators were not blinded to allocation during experiments and outcome assessment.

Extended Data

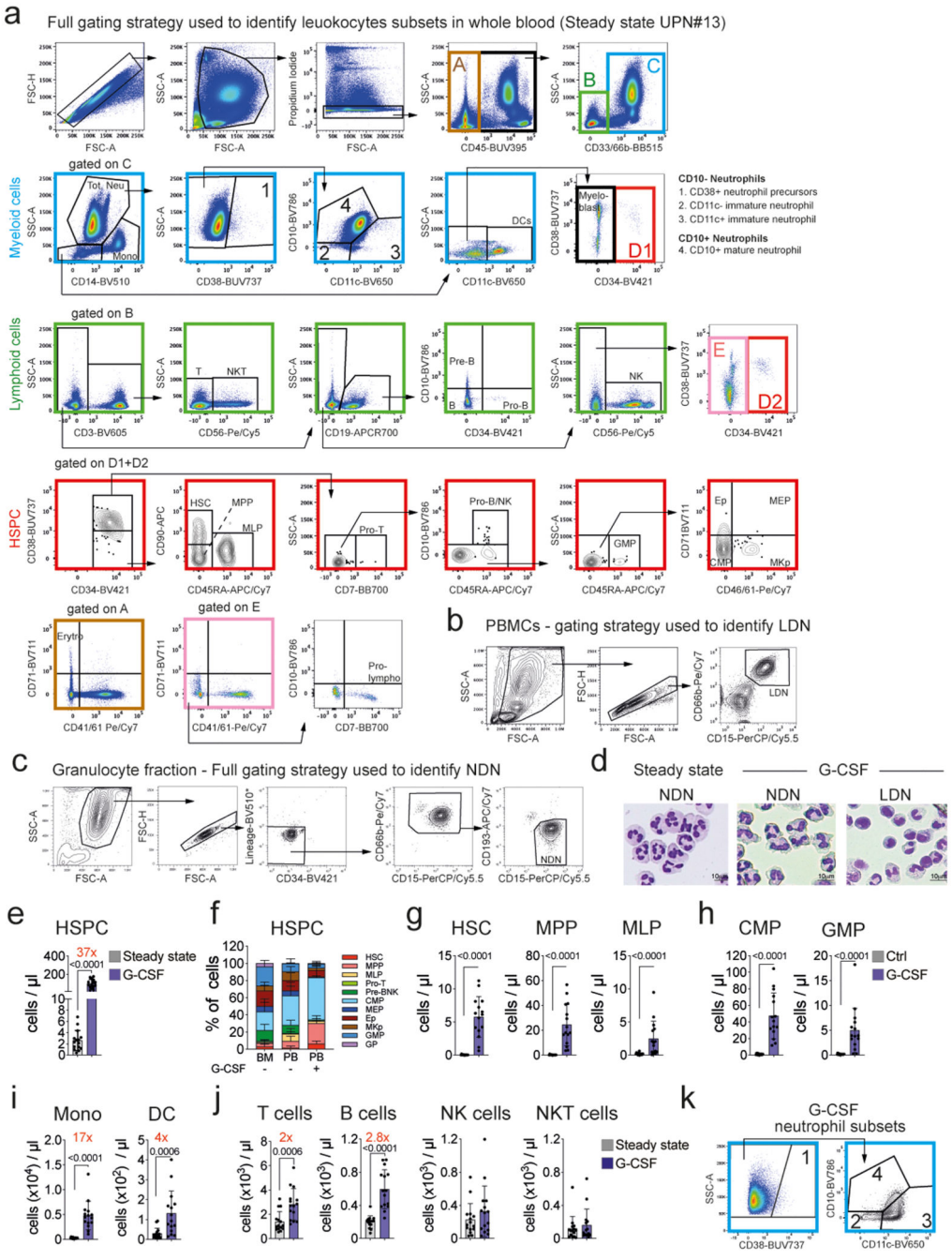

Extended Data Fig. 1. Leukocyte dynamics in G-CSF-treated donors.

a. Full gating strategy used to identify leukocytes subsets in whole PB or BM samples (blue: myeloid cells; green: lymphoid cells; red: HSPC; pink: $CD45^{+}$ $Lineage^{-}$ $CD34^{-}$ cells; brown: $CD45^{-}$ cells). Neutrophil subsets are numbered from 1 to 4 (1: SSC^{hi} $CD38^{+}$ $CD11c^{-}$ $CD10^{-}$ neutrophil precursors; 2: SSC^{hi} $CD38^{-}$ $CD11c^{-}$ $CD10^{-}$ immature neutrophils; 3: SSC^{hi} $CD38^{-}$ $CD11c^{+}$ $CD10^{-}$ immature neutrophils; 4: SSC^{hi} $CD38^{-}$ $CD11c^{-}$ $CD10^{+}$

Europe PMC Funders Author Manuscripts

mature neutrophils). **b**. Gating strategy used to identify low density neutrophils (LDNs) within PBMCs. **c**. Gating strategy used to identify normal density neutrophils (NDNs) within granulocytes. **d**. Representative May-Grunwald Giemsa staining of NDNs isolated by bead sorting (lower row) and LDN (upper row) isolated by FACS sorting from PB of healthy donors (steady state, n=3) and from G-CSF mobilized PB (n=2). **e,f.** Absolute HSPC counts in whole PB (**e**) and frequency of HSPC subsets (gated on Lin^- $CD45^+$ $CD34^+$ cells) in whole BM or PB (**f**) of controls or G-CSF-treated donors (PB n=15; BM n=14). **g-j.** Absolute counts of phenotypically defined hematopoietic stem cells (HSC), multipotent progenitors (MPP) and multi-lymphoid progenitors (MLP) (**g**), of committed common myeloid progenitors (CMP) or granulocyte-monocyte progenitors (GMP) (**h**) and of differentiated myeloid and lymphoid cells (**i,j**) in whole PB of controls or G-CSF-treated donors (n=15). **k**. Representative contour plot showing immature and mature neutrophils in the whole PB of a representative G-CSF-treated donor. Gating strategies for the indicated cell types are also reported in Supplementary Table 7. Bar plot report data as mean ± SD. Numbers in red represent fold increases in the indicated conditions. Statistical analyses. **e**, **g-j:** two-sided Mann-Whitney test.

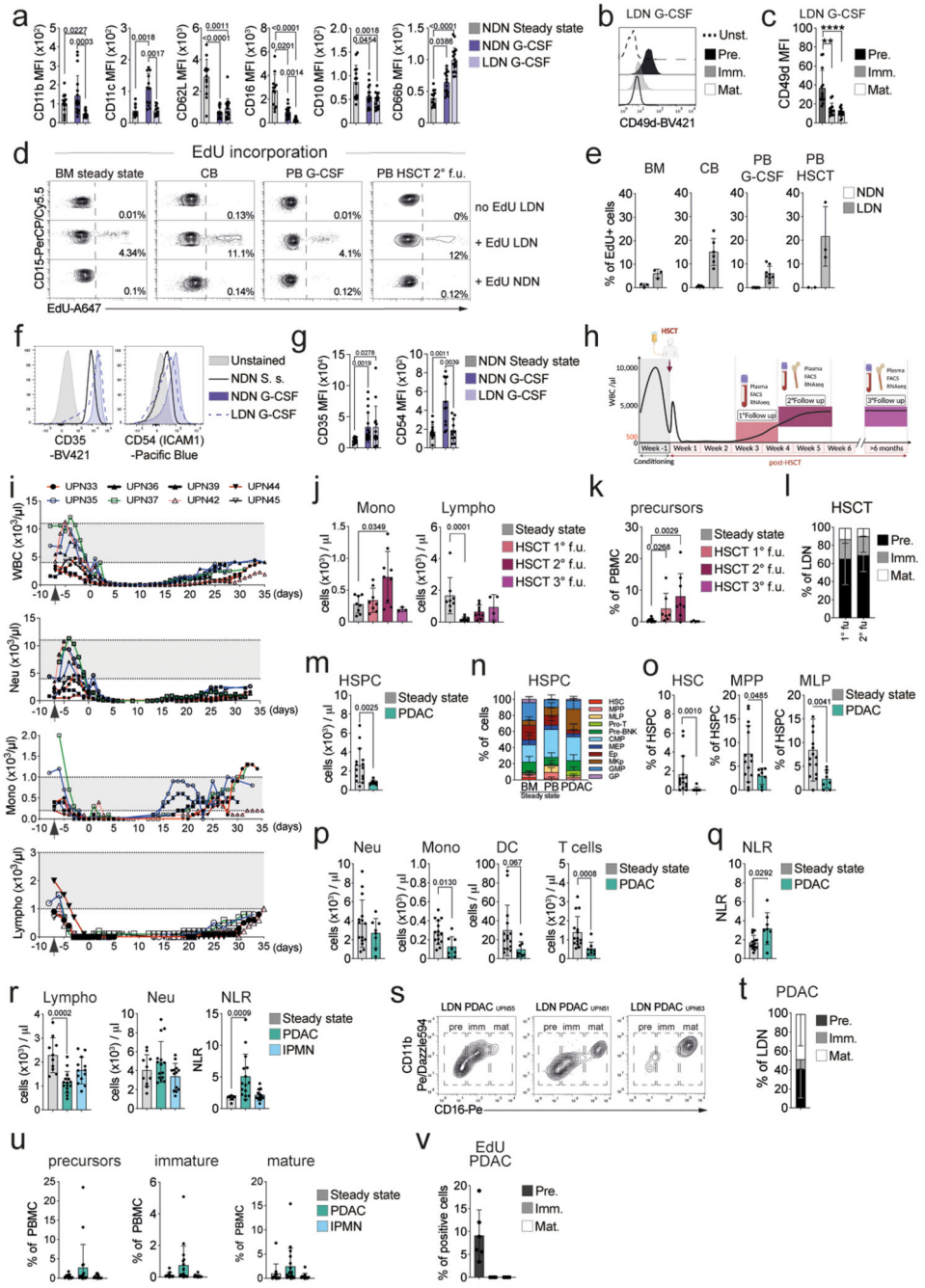

Extended Data Fig. 2. Leukocyte dynamics in HSC-T and PDAC patients.

a. Expression of the indicated markers in NDNs and LDNs from controls (n>10) or G-CSF-treated donors (n>12). **b, c**. Histogram (**b**) and cumulative histogram (**c**) plot showing the expression levels of CD49d in neutrophil precursors, immature, and mature neutrophils. **d, e**. Contour (**d**) and cumulative histogram (**e**) plots showing percentages of EdU^{+} cells within NDNs and LDNs from BM, CB and PB samples of the indicated patients (BM n=3, CB n=6, G-CSF n=8, HSCT 2° f.u. n=3). **f, g**. Representative histogram (**f**) and cumulative histogram (**g**) plot showing expression of the indicated markers in in NDNs

Europe PMC Funders Author Manuscripts

and LDNs from controls (n>11) or G-CSF-treated donors (n>11). **h**. Representation of leukocytes dynamics in HSC-T patients. **i.** Quantification of white blood cells (WBCs), neutrophil, monocyte, and lymphocyte count in HSC-T patients. Gray intervals highlight normal ranges. Arrows indicate the beginning of myeloablative conditioning; day 0 indicates the day of HSC-T. **j**. Counts of monocytes or lymphocytes in PB of controls (n=8) or HSC-T patients (1° f.u. n=8, 2° f.u. n=9, 3° f.u. n=3). **k,l**. Percentage of neutrophil precursors, immature and mature neutrophils within PBMCs (**k**) or LDNs (**l**) in controls (n=8) and HSC-T patients (1° f.u. n=7, 2° f.u. n=8). **m-o.** Absolute counts (**m**) and frequencies of HSPC subsets (**n, o**) in whole PB (n=15) or BM (n=14) of controls and PB of PDAC patients (n=8). **p.** Leukocyte counts in whole PB of controls (n=15) and PDAC patients (n=8). **q.** Neutrophil-to-lymphocyte ratio (NLR) in whole PB of controls (n=15) and PDAC (n=8) patients. NLR is calculated as the ratio between absolute counts (FACS) of neutrophils and total lymphocytes. **r.** Leukocyte counts (hemocytometer) and corresponding NLR values in whole PB of controls (n=10), IPMN (n=12) and PDAC (n=15) patients. **s**. Contour plots showing CD16 and CD11b expression in LDNs of three PDAC patients. **t, u**. Percentage of neutrophil precursors, immature and mature neutrophils within LDNs (**t**) and PBMCs (**u**) of controls (n=12), IPMN (n=12) and PDAC (n=18) patients. **v**. Percentage of EdU^+ cells within neutrophil precursors, immature and mature neutrophils in PB of PDAC patients (n=6). Gating strategies for the indicated cell types are reported in Supplementary Table 7. Bar plots report data as mean ± SD. Statistical analyses. **a, c, g, j**, **k,** and **r**: Kruskal-Wallis test plus two-sided Dunn's multiple comparison. **m, o-q:** two-sided Mann-Whitney test.

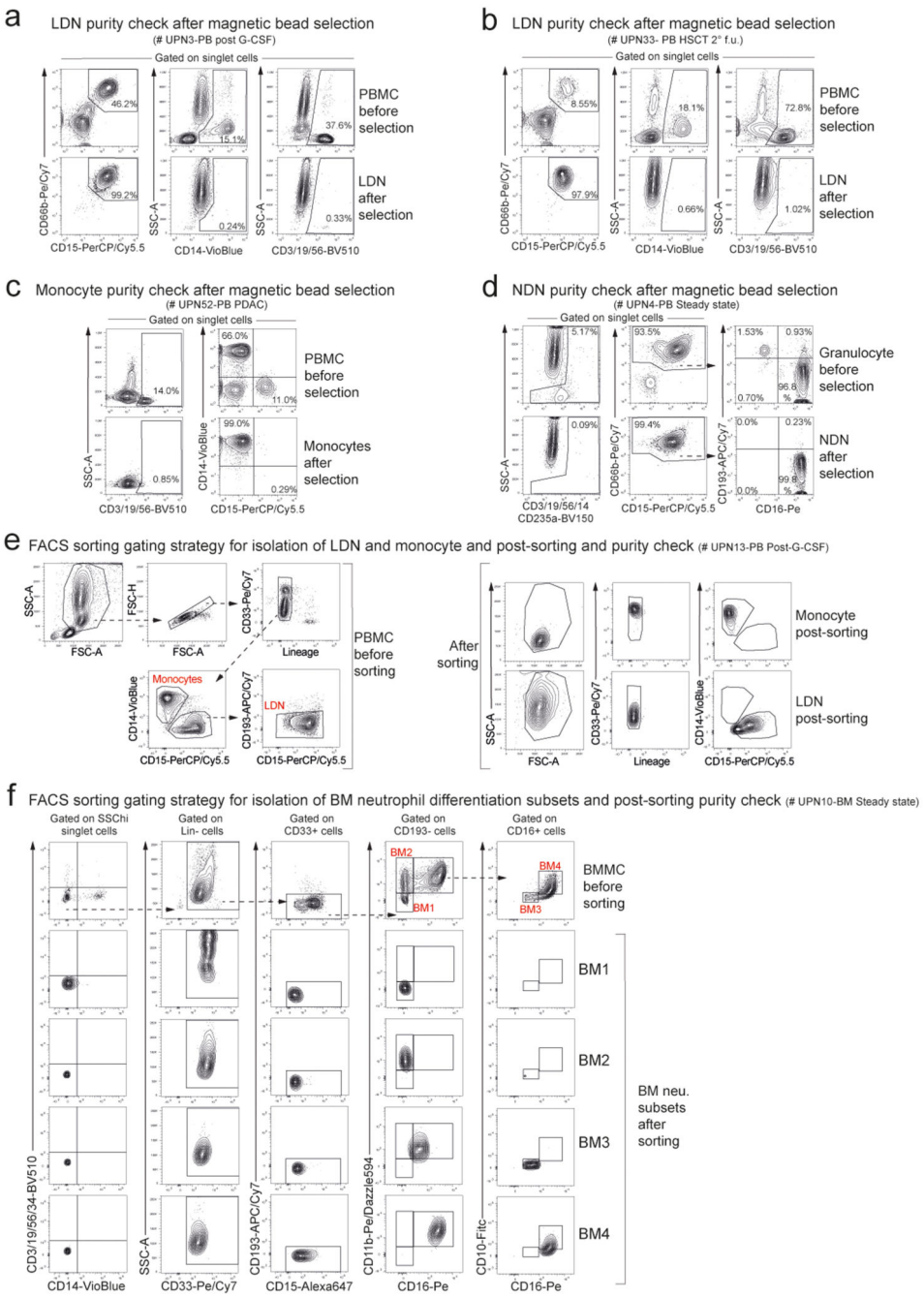

Extended Data Fig. 3. Purity of isolated cell populations.

a-d. Representative contour plots showing cell purity before and after magnetic bead selection of LDNs (**a, b**), monocytes (**c**) and NDNs (**d**) from PB samples. **e**. Representative contour plots showing the gating strategy used to isolate LDNs and monocytes (left panel) and post-sort purity analysis of sorted cells (right panel). **f**. Representative contour plots showing the gating strategy used to isolate BM neutrophil subsets and post-sort purity analysis of sorted cells.

Europe PMC Funders Author Manuscripts

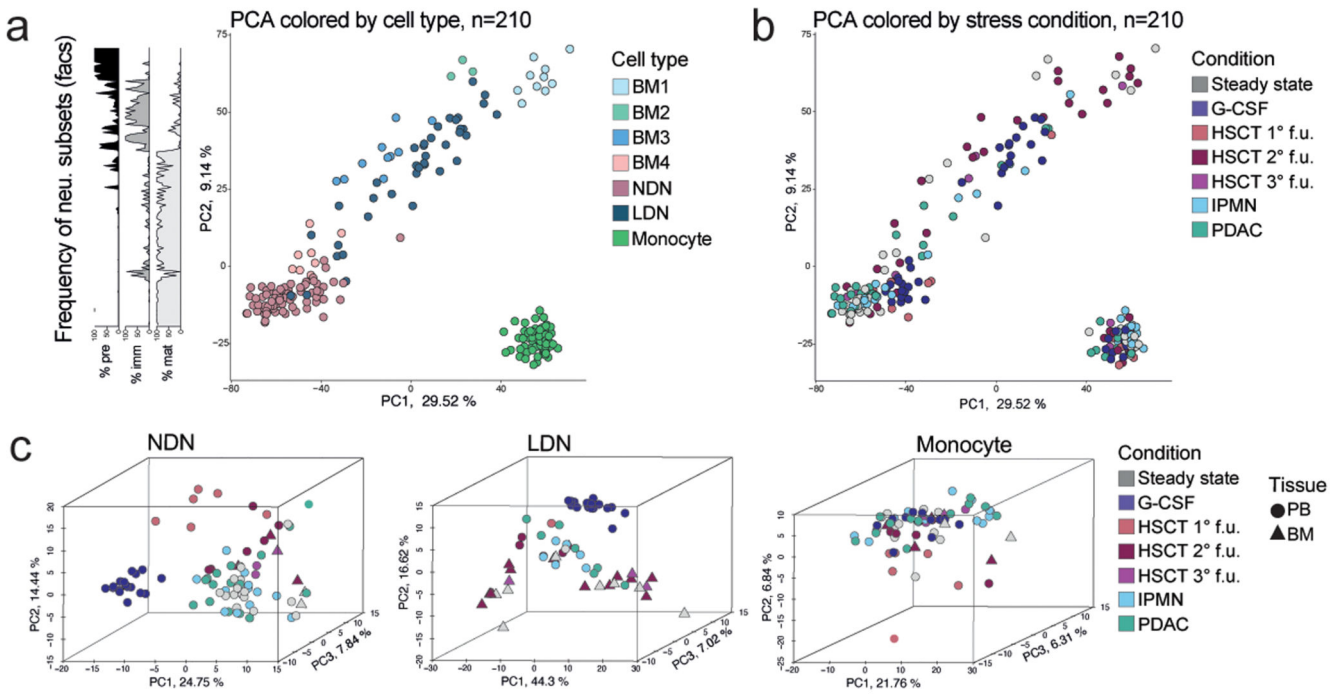

Extended Data Fig. 4. Bulk RNA-Seq analysis of NDNs, LDNs, and monocytes.

a, b. Principal component analysis (PCA) plots of bulk RNA-Seq datasets of NDNs, LDNs and monocytes isolated from PB of healthy controls (n=19), G-CSF-treated donors (n=17), HSC-T (n=8), PDAC (n=15) and IPMN (n=14) patients, as well as of neutrophil differentiation intermediates from BM of healthy donors (n=3) and HSCT patients (n=7). Samples are colored based on cell type (**a**) or stress condition (**b**), as indicated by the legends. Filled area plot on the left show the frequency of neutrophil precursors (pre), immature (imm) and mature (mat) neutrophils for the corresponding NDNs and LDNs samples along PC2. **c.** PCA plots of bulk RNA-Seq datasets of NDNs, LDNs or monocytes. Colors represent stress condition, while shapes reflect the tissue of origin (PB circle; BM triangle), as indicated in the legend.

Europe PMC Funders Author Manuscripts

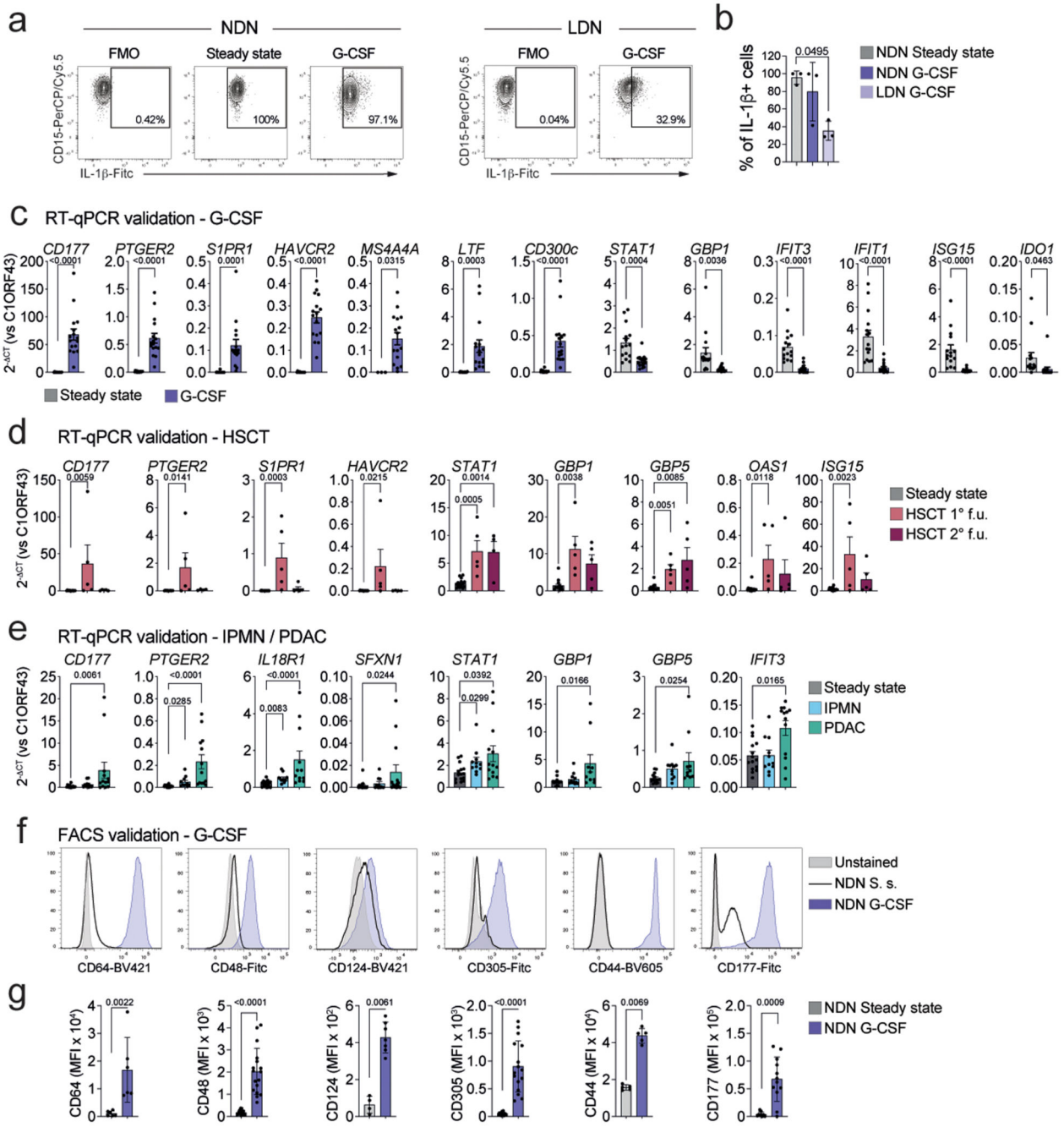

Extended Data Fig. 5. Validation of RNA-Seq analyses in NDNs.

a, b. Representative contour plots (**a**) and cumulative bar plot (**b**) showing the basal expression of IL-1β in NDNs and LDNs isolated from controls (n=3) and G-CSF treated donors (n=3). **c-e**. Cumulative bar plots showing the expression of the indicated genes in NDNs isolated from controls and G-CSF treated donors (**c**), HSC-T patients (**d**) or IPMN and PDAC patients (**e**). **f,g**. Representative histogram plots (**f**) and cumulative histogram plots (**g**) showing the expression of the indicated markers in NDNs isolated from PB of controls (n>5) and G-CSF-treated donors (n>5). Bar plots report data as mean ± SD.

Statistical analyses. **c** and **g:** two-sided Mann-Whitney test. **b, d** and **e** Kruskal-Wallis test plus two-sided Dunn's multiple comparison.

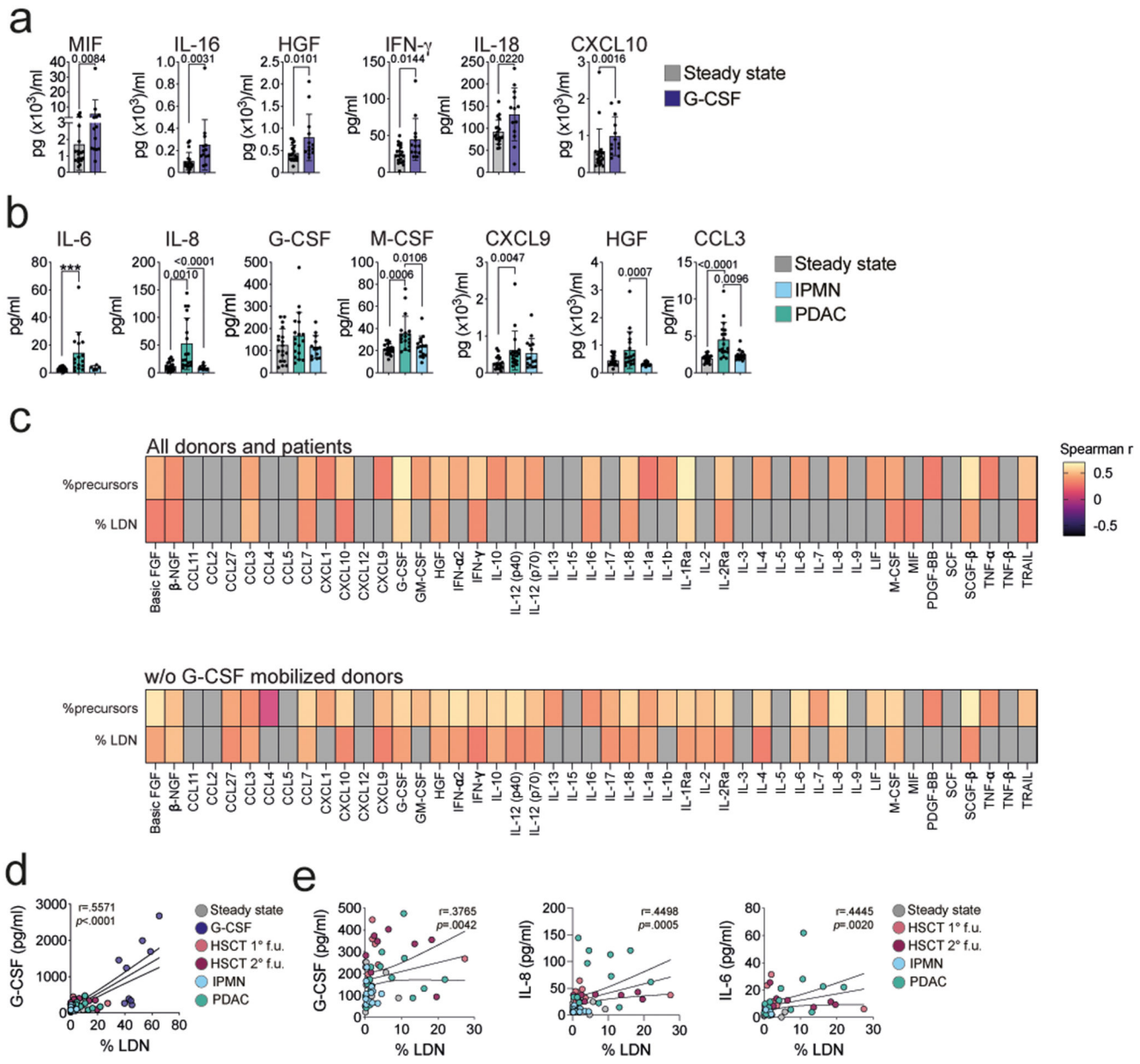

Extended Data Fig. 6. Plasma factors in G-CSF-treated donors, HSC-T or PDAC patients.

a,b. Concentration of selected factors in the plasma of controls (n=19) and G-CSF-treated donors (n=13) (**a**) or controls (n=19) and IPMN (n=15) or PDAC (n=18) patients (**b**).

c. Correlation between plasma concentrations of the indicated factor and frequencies of neutrophils precursors or LDNs in the PMBC fraction. Colors indicate calculated Spearman's correlation coefficients (p-value < 0.05). Gray, not significant. Data are shown for all experimental conditions (upper heatmap) or excluding G-CSF-treated donors (lower heatmap) (steady state n= 14; G-CSF n=9; HSCT 1° f.u. n=7; HSCT 2° f.u. n=8; IPMN

Europe PMC Funders Author Manuscripts

n=14; PDAC n=16) **d, e**. Correlation between plasma concentrations of the indicated factor and frequencies of LDNs in the PMBC fraction combining all samples together (**d**) or excluding (**e**) G-CSF-treated donors. Spearman's correlation and p-values are shown for each plot. Bar plots report data as mean ± SD Statistical analyses. **a**: two-sided Mann-Whitney test; **b**: Kruskal-Wallis test plus two-sided Dunn's multiple comparison; **c-e**: Spearman's correlation.

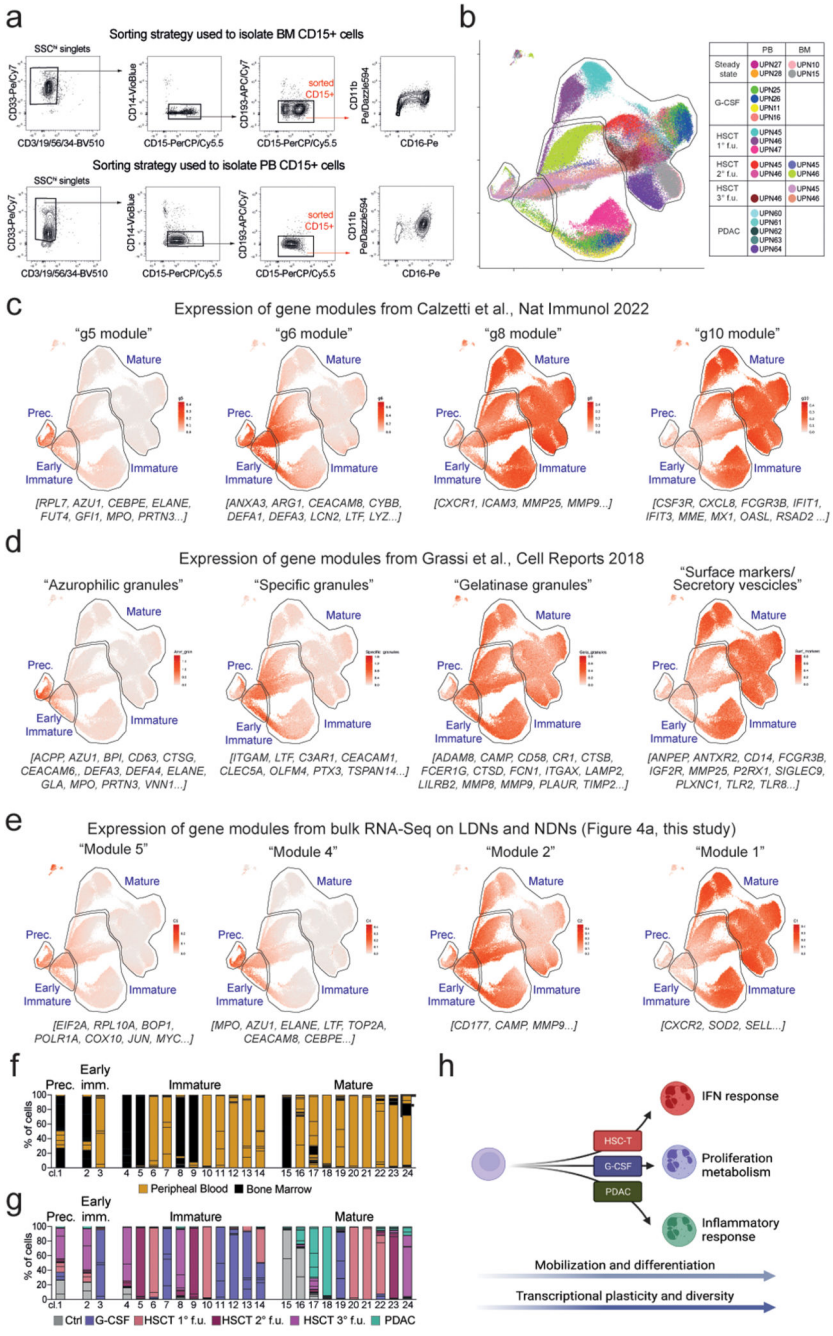

Extended Data Fig. 7. Single-cell RNA-Seq analyses of human neutrophils.

Europe PMC Funders Author Manuscripts

a. Gating strategy used to isolate $CD15^+$ neutrophils from whole BM (upper panel) or PB (lower panel) samples. Expression of CD16 and CD11b in sorted cells is shown. **b**. UMAP plot showing donor or patient identities. **c-d**. UMAP plots showing the expression of gene modules related to neutrophil maturation identified in the indicated studies. **e**. UMAP plots showing the expression of gene modules identified from bulk RNA-Seq analysis (see Fig. 4a and Supplementary Table 9). **f, g**. Stacked bar plots showing the frequency of cells from PB or BM samples (**f**) or from donors and patients (**g**) for each neutrophil cluster. **h.** Model depicting divergent developmental trajectories in stress-elicited neutrophils, leading to diverse gene expression programs of mature cells.

Europe PMC Funders Author Manuscripts

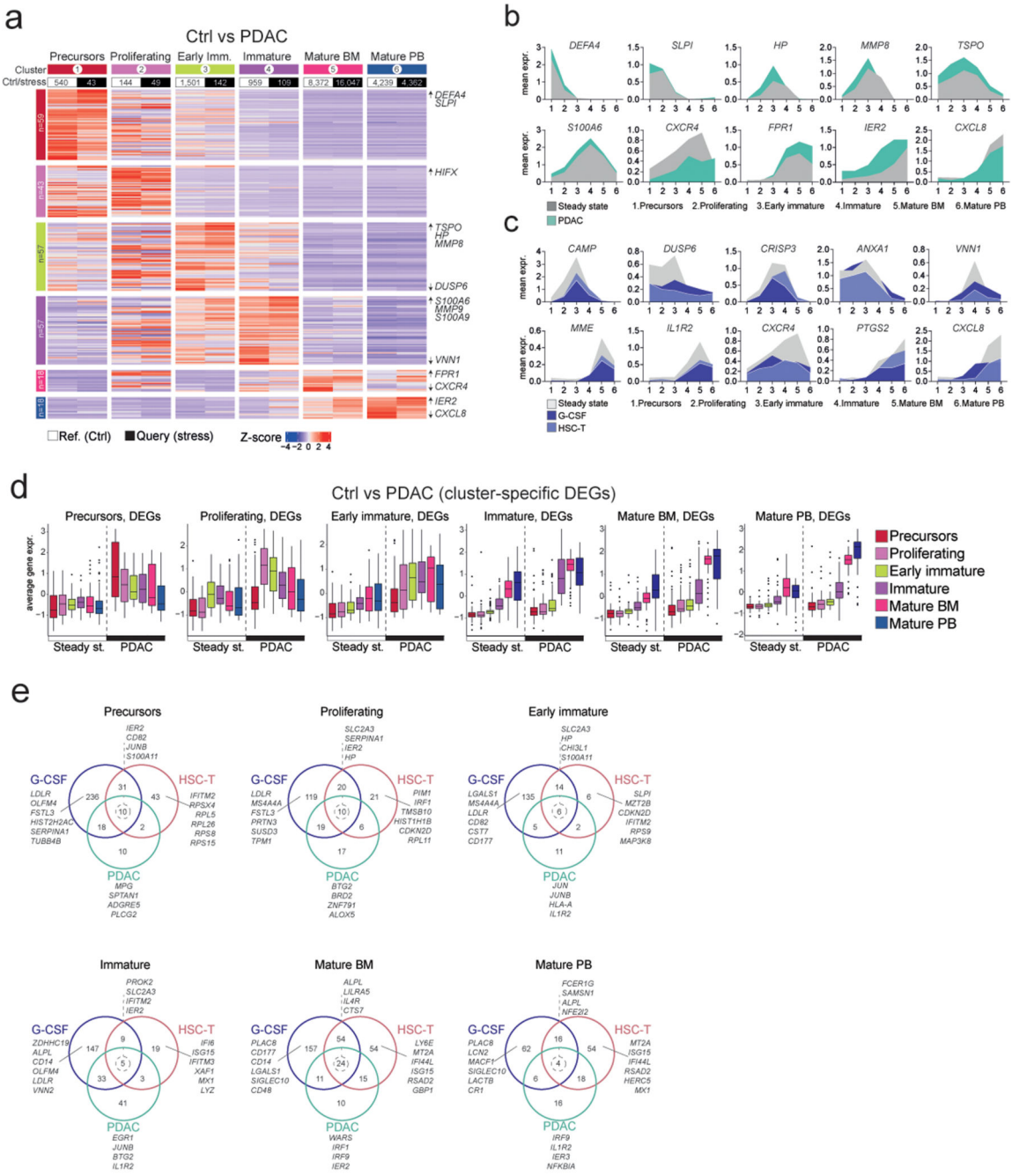

Extended Data Fig. 8. CellHarmony analyses of neutrophils from G-CSF-treated donors, HSC-T or PDAC patients.

a. Heatmap showing standardized average expression (computed on normalized expression levels) of developmental marker genes identified by Cell Harmony and expressed in at least 20% of cells from reference datasets for the indicated neutrophil subsets in controls (reference, white bars) and PDAC patients (query, black bars). Color bars represent stages of neutrophil development after alignment of scRNA-Seq data with Cell Harmony. The number of cells from reference and query datasets for each cluster is shown at the top, the number

Europe PMC Funders Author Manuscripts

Europe PMC Funders Author Manuscripts

of developmental marker genes for each cluster is shown on the left. Selected representative genes are highlighted on the right. **b, c.** Filled area plots showing mean expression in scRNA-Seq data of selected developmental marker genes in neutrophil subsets from controls (grey) and PDAC (green) (**b**) or controls and G-CSF-treated donors (dark blue) or HSC-T patients (light blue) (**c**). Numbers on the x-axis indicate the stages of neutrophil development identified by Cell Harmony. **d**. Box plots showing standardized average expression of genes up regulated (see Methods) in the indicated neutrophil subsets from PDAC patients versus controls. Each plot refers to induced genes in query versus reference scRNA-Seq datasets for neutrophils at each stage of development defined by Cell Harmony. Box plots represent the median, interquartile range (IQR), minimum (25th percentile, 1.5 × IQR) and maximum (75th percentile, 1.5 × IQR). Sample size corresponds to the number of cells indicated in the heatmap (**a**). **e.** Venn diagram showing the overlap between up-regulated genes in G-CSF treated donors and HSC-T and PDAC patients in the indicated stages of neutrophil development. A selection of genes up-regulated in all conditions and of stress-specific genes are shown (see Supplementary Table 37).

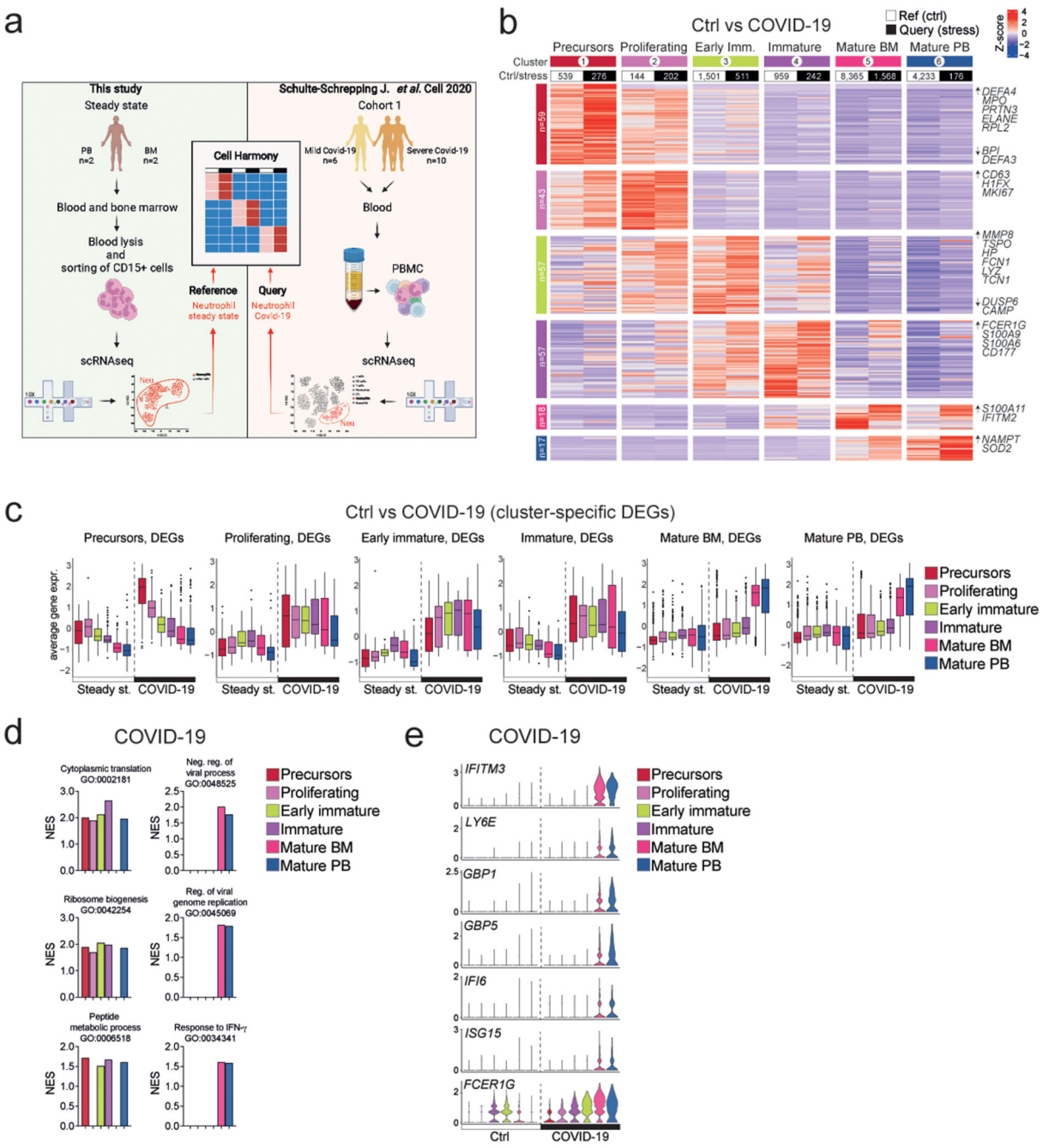

Extended Data Fig. 9. CellHarmony analyses of neutrophils from COVID-19 patients.

a. Scheme depicting the experimental and computational strategies used to isolate and process for scRNAseq analysis cells from controls and COVID-19 patients. **b**. Heatmap showing standardized average expression (computed on normalized expression levels) of developmental marker genes identified by Cell Harmony and expressed in at least 20% of cells from reference datasets for the indicated neutrophil subsets in controls (reference, white bars) and COVID-19 patients (query, black bars). Color bars represent stages of neutrophil development after alignment of scRNA-Seq data with Cell Harmony. The number

Europe PMC Funders Author Manuscripts

of cells from reference and query datasets for each cluster is shown at the top, the number of developmental marker genes for each cluster is shown on the left. Selected representative genes are highlighted on the right. **c**. Box plots showing standardized average expression of genes up regulated (see Methods) in the indicated neutrophil subsets from COVID-19 patients versus controls. Each plot refers to induced genes in query versus reference scRNA-Seq datasets for neutrophils at each stage of development defined by Cell Harmony. Box plots represent the median, interquartile range (IQR), minimum (25th percentile, 1.5 × IQR) and maximum (75th percentile, 1.5 × IQR). Sample size corresponds to the number of cells indicated in the heatmap (**b**). **d.** Bar plots showing NES of selected GO categories enriched within genes expressed at higher levels in neutrophil subsets from COVID-19 patients as compared to controls. Colors represent stages of neutrophil development defined by Cell Harmony. **e.** Violin plots showing normalized expression levels of selected genes induced in mature neutrophils from COVID-19 patients as compared to controls. Colors represent stages of neutrophil development defined by Cell Harmony.

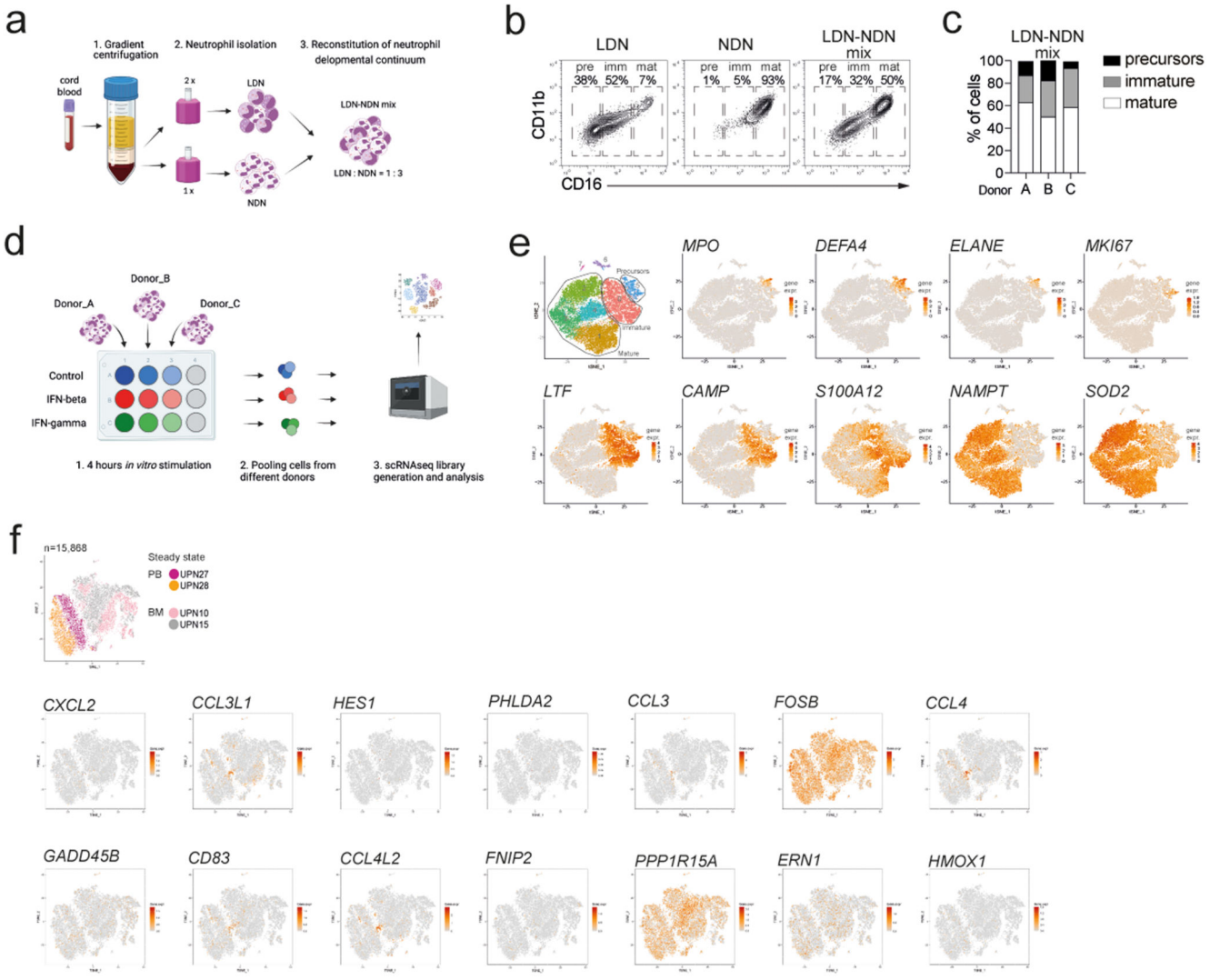

Europe PMC Funders Author Manuscripts

Extended Data Fig. 10. Single-cell RNA-Seq analysis of IFN-stimulated neutrophils.
a. Experimental strategy used to enrich and mix LDNs and NDNs from CB samples, ensuring a sufficient representation of all neutrophil subsets (see Methods). **b, c.** Representative contour plots (**b**) and stacked bar plot (**c**) showing the percentage of neutrophil precursors (pre), immature (imm) and mature (mat) neutrophils in LDN, NDN and LDN-NDN mix (1:3). **d.** Schematic representation of CB neutrophil stimulation and processing for scRNA-Seq analysis. **e.** tSNE plots showing the expression of selected developmental marker genes. **f.** tSNE plots showing expression of cluster 3 marker genes (corresponding to CB neutrophils) in PB and BM neutrophils from steady-state controls.

Supplementary Material

Refer to Web version on PubMed Central for supplementary material.

Acknowledgements

We thank S. Gregori and G. Amodio for help with neutrophil isolation and culture experiments; F. Di Salvo, F. Porzio and M. Tassara for patient recruitment and data management; the Center for Omics Sciences (COSR), the Flow cytometry Resource, Advanced Cytometry Technical Applications Laboratory (FRACTAL), Centro Risorse Biologiche (CRB-OSR) at Ospedale San Raffaele; the Centro Universitario di Statistica per le Scienze Biomediche (CUSSB) at Vita-Salute San Raffaele University. Figures were created with Adobe Illustrator and BioRender.com. V.B. and F.V.M. conducted this study as partial fulfilment of a PhD in Molecular Medicine (Basic and Applied Immunology and Oncology program) at Vita-Salute San Raffaele University. R.D.M. is a New York Stem Cell Foundation – Robertson Investigator. M.A.C. and P.S. are supported by grants from the Italian Association for Cancer Research (AIRC) (IG 20339) and the Italian Ministry of University and Research (PRIN 20177J4E75_004). A.A is supported by the Italian Telethon Foundation (SR-Tiget Grant Award B02). E.M. and N.C. are supported by fellowships from Fondazione Umberto Veronesi (FUV). This study was supported by grants from the Italian Telethon Foundation (SR-Tiget Grant Award F04 to R.O) and the Italian Ministry of Health (GR-201602362156 to R.O. and S.C.). Research in the R.O. lab is supported by the European Research Council (ERC) (ERC Starting Grant 759532, X-TAM) and by AIRC (MFAG 20247 and AIRC 5x1000 special program 22737).

Data Availability

Bulk and single-cell RNA-Seq data generated in this study have been deposited in ArrayExpress under the accession numbers E-MTAB-11190 and E-MTAB-11188. Single cell RNA-seq data of COVID-19 patients[27] were downloaded from FASTGenomics database at https://beta.fastgenomics.org/datasets/detail-dataset-7656cfe94fb14a01b787f4774e555036. Source data are provided with this paper.

References

1. Ley K, et al. Neutrophils: New insights and open questions. Sci Immunol. 2018; 3 doi: 10.1126/sciimmunol.aat4579
2. Skokowa J, Dale DC, Touw IP, Zeidler C, Welte K. Severe congenital neutropenias. Nat Rev Dis Primers. 2017; 3 17032 doi: 10.1038/nrdp.2017.32 [PubMed: 28593997]
3. Copelan EA. Hematopoietic stem-cell transplantation. N Engl J Med. 2006; 354: 1813–1826. DOI: 10.1056/NEJMra052638 [PubMed: 16641398]
4. Jaillon S, et al. Neutrophil diversity and plasticity in tumour progression and therapy. Nat Rev Cancer. 2020; 20: 485–503. DOI: 10.1038/s41568-020-0281-y [PubMed: 32694624]
5. Ng LG, Ostuni R, Hidalgo A. Heterogeneity of neutrophils. Nat Rev Immunol. 2019; 19: 255–265. DOI: 10.1038/s41577-019-0141-8 [PubMed: 30816340]
6. Ballesteros I, et al. Co-option of Neutrophil Fates by Tissue Environments. Cell. 2020; 183: 1282–1297. e1218 doi: 10.1016/j.cell.2020.10.003 [PubMed: 33098771]

7. Casanova-Acebes M, et al. Rhythmic modulation of the hematopoietic niche through neutrophil clearance. Cell. 2013; 153: 1025–1035. DOI: 10.1016/j.cell.2013.04.040 [PubMed: 23706740]
8. Manz MG, Boettcher S. Emergency granulopoiesis. Nat Rev Immunol. 2014; 14: 302–314. DOI: 10.1038/nri3660 [PubMed: 24751955]
9. Kwok I, et al. Combinatorial Single-Cell Analyses of Granulocyte-Monocyte Progenitor Heterogeneity Reveals an Early Uni-potent Neutrophil Progenitor. Immunity. 2020; 53: 303–318. e305 doi: 10.1016/j.immuni.2020.06.005 [PubMed: 32579887]
10. Evrard M, et al. Developmental Analysis of Bone Marrow Neutrophils Reveals Populations Specialized in Expansion, Trafficking, and Effector Functions. Immunity. 2018; 48: 364–379. e368 doi: 10.1016/j.immuni.2018.02.002 [PubMed: 29466759]
11. Dinh HQ, et al. Coexpression of CD71 and CD117 Identifies an Early Unipotent Neutrophil Progenitor Population in Human Bone Marrow. Immunity. 2020; 53: 319–334. e316 doi: 10.1016/j.immuni.2020.07.017 [PubMed: 32814027]
12. Zilionis R, et al. Single-Cell Transcriptomics of Human and Mouse Lung Cancers Reveals Conserved Myeloid Populations across Individuals and Species. Immunity. 2019; 50: 1317–1334. e1310 doi: 10.1016/j.immuni.2019.03.009 [PubMed: 30979687]
13. Calcagno DM, et al. The myeloid type I interferon response to myocardial infarction begins in bone marrow and is regulated by Nrf2-activated macrophages. Sci Immunol. 2020; 5 doi: 10.1126/sciimmunol.aaz1974
14. Xie X, et al. Single-cell transcriptome profiling reveals neutrophil heterogeneity in homeostasis and infection. Nat Immunol. 2020; 21: 1119–1133. DOI: 10.1038/s41590-020-0736-z [PubMed: 32719519]
15. Zhu YP, et al. CyTOF mass cytometry reveals phenotypically distinct human blood neutrophil populations differentially correlated with melanoma stage. J Immunother Cancer. 2020; 8 doi: 10.1136/jitc-2019-000473
16. Khoyratty TE, et al. Distinct transcription factor networks control neutrophil-driven inflammation. Nat Immunol. 2021; 22: 1093–1106. DOI: 10.1038/s41590-021-00968-4 [PubMed: 34282331]
17. Basso-Ricci L, et al. Multiparametric Whole Blood Dissection: A one-shot comprehensive picture of the human hematopoietic system. Cytometry A. 2017; 91: 952–965. DOI: 10.1002/cyto.a.23148 [PubMed: 28609016]
18. Pedersen CC, et al. Changes in Gene Expression during G-CSF-Induced Emergency Granulopoiesis in Humans. J Immunol. 2016; 197: 1989–1999. DOI: 10.4049/jimmunol.1502690 [PubMed: 27481851]
19. Marini O, et al. Mature CD10(+) and immature CD10(-) neutrophils present in G-CSF-treated donors display opposite effects on T cells. Blood. 2017; 129: 1343–1356. DOI: 10.1182/blood-2016-04-713206 [PubMed: 28053192]
20. Crippa S, et al. Low progression of intraductal papillary mucinous neoplasms with worrisome features and high-risk stigmata undergoing non-operative management: a mid-term follow-up analysis. Gut. 2017; 66: 495–506. DOI: 10.1136/gutjnl-2015-310162 [PubMed: 26743012]
21. Howard R, Kanetsky PA, Egan KM. Exploring the prognostic value of the neutrophil-to-lymphocyte ratio in cancer. Sci Rep. 2019; 9 19673 doi: 10.1038/s41598-019-56218-z [PubMed: 31873162]
22. Zhang J, et al. CD13(hi) Neutrophil-like myeloid-derived suppressor cells exert immune suppression through Arginase 1 expression in pancreatic ductal adenocarcinoma. Oncoimmunology. 2017; 6 e1258504 doi: 10.1080/2162402X.2016.1258504 [PubMed: 28344866]
23. Tamassia N, et al. Induction of OCT2 contributes to regulate the gene expression program in human neutrophils activated via TLR8. Cell Rep. 2021; 35 109143 doi: 10.1016/j.celrep.2021.109143 [PubMed: 34010659]
24. Grassi L, et al. Dynamics of Transcription Regulation in Human Bone Marrow Myeloid Differentiation to Mature Blood Neutrophils. Cell Rep. 2018; 24: 2784–2794. DOI: 10.1016/j.celrep.2018.08.018 [PubMed: 30184510]
25. Calzetti F, et al. CD66b(-)CD64(dim)CD115(-) cells in the human bone marrow represent neutrophil-committed progenitors. Nat Immunol. 2022; 23: 679–691. DOI: 10.1038/s41590-022-01189-z [PubMed: 35484408]

26. DePasquale EAK, et al. cellHarmony: cell-level matching and holistic comparison of single-cell transcriptomes. Nucleic Acids Res. 2019; 47: e138. doi: 10.1093/nar/gkz789 [PubMed: 31529053]
27. Schulte-Schrepping J, et al. Severe COVID-19 Is Marked by a Dysregulated Myeloid Cell Compartment. Cell. 2020; 182: 1419–1440. e1423 doi: 10.1016/j.cell.2020.08.001 [PubMed: 32810438]
28. Silvin A, et al. Elevated Calprotectin and Abnormal Myeloid Cell Subsets Discriminate Severe from Mild COVID-19. Cell. 2020; 182: 1401–1418. e1418 doi: 10.1016/j.cell.2020.08.002 [PubMed: 32810439]
29. Grieshaber-Bouyer R, et al. The neutrotime transcriptional signature defines a single continuum of neutrophils across biological compartments. Nat Commun. 2021; 12 2856 doi: 10.1038/s41467-021-22973-9 [PubMed: 34001893]
30. Muench DE, et al. Mouse models of neutropenia reveal progenitor-stage-specific defects. Nature. 2020; 582: 109–114. DOI: 10.1038/s41586-020-2227-7 [PubMed: 32494068]
31. Alshetaiwi H, et al. Defining the emergence of myeloid-derived suppressor cells in breast cancer using single-cell transcriptomics. Sci Immunol. 2020; 5 doi: 10.1126/sciimmunol.aay6017
32. Hoggatt J, et al. Rapid Mobilization Reveals a Highly Engraftable Hematopoietic Stem Cell. Cell. 2018; 172: 191–204. e110 doi: 10.1016/j.cell.2017.11.003 [PubMed: 29224778]
33. Bowers E, et al. Granulocyte-derived TNFalpha promotes vascular and hematopoietic regeneration in the bone marrow. Nat Med. 2018; 24: 95–102. DOI: 10.1038/nm.4448 [PubMed: 29155425]
34. Shaul ME, Fridlender ZG. Tumour-associated neutrophils in patients with cancer. Nat Rev Clin Oncol. 2019; 16: 601–620. DOI: 10.1038/s41571-019-0222-4 [PubMed: 31160735]
35. Quail DF, et al. Neutrophil phenotypes and functions in cancer: A consensus statement. J Exp Med. 2022; 219 doi: 10.1084/jem.20220011
36. Cassatella MA, Scapini P. On the Improper Use of the Term High-Density Neutrophils. Trends Immunol. 2020; 41: 1059–1061. DOI: 10.1016/j.it.2020.10.008 [PubMed: 33160842]
37. Veglia F, Sanseviero E, Gabrilovich DI. Myeloid-derived suppressor cells in the era of increasing myeloid cell diversity. Nat Rev Immunol. 2021; 21: 485–498. DOI: 10.1038/s41577-020-00490-y [PubMed: 33526920]
38. Natoli G, Ostuni R. Adaptation and memory in immune responses. Nat Immunol. 2019; 20: 783–792. DOI: 10.1038/s41590-019-0399-9 [PubMed: 31213714]
39. Kalafati L, et al. Innate Immune Training of Granulopoiesis Promotes Anti-tumor Activity. Cell. 2020; 183: 771–785. e712 doi: 10.1016/j.cell.2020.09.058 [PubMed: 33125892]
40. Moorlag S, et al. BCG Vaccination Induces Long-Term Functional Reprogramming of Human Neutrophils. Cell Rep. 2020; 33 108387 doi: 10.1016/j.celrep.2020.108387 [PubMed: 33207187]
41. Hill GR, Koyama M. Cytokines and costimulation in acute graft-versus-host disease. Blood. 2020; 136: 418–428. DOI: 10.1182/blood.2019000952 [PubMed: 32526028]
42. Tomblyn M, et al. Guidelines for preventing infectious complications among hematopoietic cell transplantation recipients: a global perspective. Biol Blood Marrow Transplant. 2009; 15: 1143–1238. DOI: 10.1016/j.bbmt.2009.06.019 [PubMed: 19747629]
43. Tamassia N, et al. Cutting edge: An inactive chromatin configuration at the IL-10 locus in human neutrophils. J Immunol. 2013; 190: 1921–1925. DOI: 10.4049/jimmunol.1203022 [PubMed: 23355741]
44. Tamassia N, et al. The MyD88-independent pathway is not mobilized in human neutrophils stimulated via TLR4. J Immunol. 2007; 178: 7344–7356. DOI: 10.4049/jimmunol.178.11.7344 [PubMed: 17513785]
45. Berry MP, et al. An interferon-inducible neutrophil-driven blood transcriptional signature in human tuberculosis. Nature. 2010; 466: 973–977. DOI: 10.1038/nature09247 [PubMed: 20725040]
46. Dunning J, et al. Progression of whole-blood transcriptional signatures from interferon-induced to neutrophil-associated patterns in severe influenza. Nat Immunol. 2018; 19: 625–635. DOI: 10.1038/s41590-018-0111-5 [PubMed: 29777224]
47. Aschenbrenner AC, et al. Disease severity-specific neutrophil signatures in blood transcriptomes stratify COVID-19 patients. Genome Med. 2021; 13: 7. doi: 10.1186/s13073-020-00823-5 [PubMed: 33441124]

Europe PMC Funders Author Manuscripts

48. Song D, et al. A cellular census of human peripheral immune cells identifies novel cell states in lung diseases. Clin Transl Med. 2021; 11: e579. doi: 10.1002/ctm2.579 [PubMed: 34841705]
49. Bost P, et al. Deciphering the state of immune silence in fatal COVID-19 patients. Nat Commun. 2021; 12 1428 doi: 10.1038/s41467-021-21702-6 [PubMed: 33674591]
50. Hsu BE, et al. Immature Low-Density Neutrophils Exhibit Metabolic Flexibility that Facilitates Breast Cancer Liver Metastasis. Cell Rep. 2019; 27: 3902–3915. e3906 doi: 10.1016/j.celrep.2019.05.091 [PubMed: 31242422]
51. Serra MC, Calzetti F, Ceska M, Cassatella MA. Effect of substance P on superoxide anion and IL-8 production by human PMNL. Immunology. 1994; 82: 63–69. [PubMed: 7519174]
52. Picelli S, et al. Full-length RNA-seq from single cells using Smart-seq2. Nat Protoc. 2014; 9: 171–181. DOI: 10.1038/nprot.2014.006 [PubMed: 24385147]
53. Dobin A, et al. STAR: ultrafast universal RNA-seq aligner. Bioinformatics. 2013; 29: 15–21. DOI: 10.1093/bioinformatics/bts635 [PubMed: 23104886]
54. Liao Y, Smyth GK, Shi W. The R package Rsubread is easier, faster, cheaper and better for alignment and quantification of RNA sequencing reads. Nucleic Acids Res. 2019; 47: e47. doi: 10.1093/nar/gkz114 [PubMed: 30783653]
55. Robinson MD, McCarthy DJ, Smyth GK. edgeR: a Bioconductor package for differential expression analysis of digital gene expression data. Bioinformatics. 2010; 26: 139–140. DOI: 10.1093/bioinformatics/btp616 [PubMed: 19910308]
56. Robinson MD, Oshlack A. A scaling normalization method for differential expression analysis of RNA-seq data. Genome Biol. 2010; 11 R25 doi: 10.1186/gb-2010-11-3-r25 [PubMed: 20196867]
57. Robinson MD, Smyth GK. Moderated statistical tests for assessing differences in tag abundance. Bioinformatics. 2007; 23: 2881–2887. DOI: 10.1093/bioinformatics/btm453 [PubMed: 17881408]
58. McCarthy DJ, Chen Y, Smyth GK. Differential expression analysis of multifactor RNA-Seq experiments with respect to biological variation. Nucleic Acids Res. 2012; 40: 4288–4297. DOI: 10.1093/nar/gks042 [PubMed: 22287627]
59. Zhang Y, Parmigiani G, Johnson WE. ComBat-seq: batch effect adjustment for RNA-seq count data. NAR Genom Bioinform. 2020; 2 lqaa078 doi: 10.1093/nargab/lqaa078 [PubMed: 33015620]
60. Leek JT, Johnson WE, Parker HS, Jaffe AE, Storey JD. The sva package for removing batch effects and other unwanted variation in high-throughput experiments. Bioinformatics. 2012; 28: 882–883. DOI: 10.1093/bioinformatics/bts034 [PubMed: 22257669]
61. Phipson B, Lee S, Majewski IJ, Alexander WS, Smyth GK. Robust Hyperparameter Estimation Protects against Hypervariable Genes and Improves Power to Detect Differential Expression. Ann Appl Stat. 2016; 10: 946–963. DOI: 10.1214/16-AOAS920 [PubMed: 28367255]
62. Lun AT, Chen Y, Smyth GK. It's DE-licious: A Recipe for Differential Expression Analyses of RNA-seq Experiments Using Quasi-Likelihood Methods in edgeR. Methods Mol Biol. 2016; 1418: 391–416. DOI: 10.1007/978-1-4939-3578-9_19 [PubMed: 27008025]
63. Lund SP, Nettleton D, McCarthy DJ, Smyth GK. Detecting differential expression in RNA-sequence data using quasi-likelihood with shrunken dispersion estimates. Stat Appl Genet Mol Biol. 2012; 11 doi: 10.1515/1544-6115.1826
64. Subramanian A, et al. Gene set enrichment analysis: a knowledge-based approach for interpreting genome-wide expression profiles. Proc Natl Acad Sci US A. 2005; 102: 15545–15550. DOI: 10.1073/pnas.0506580102
65. Luecken MD, Theis FJ. Current best practices in single-cell RNA-seq analysis: a tutorial. Mol Syst Biol. 2019; 15 e8746 doi: 10.15252/msb.20188746 [PubMed: 31217225]
66. Hafemeister C, Satija R. Normalization and variance stabilization of single-cell RNA-seq data using regularized negative binomial regression. Genome Biol. 2019; 20: 296. doi: 10.1186/s13059-019-1874-1 [PubMed: 31870423]
67. Becht E, et al. Dimensionality reduction for visualizing single-cell data using UMAP. Nat Biotechnol. 2018; doi: 10.1038/nbt.4314
68. Finak G, et al. MAST: a flexible statistical framework for assessing transcriptional changes and characterizing heterogeneity in single-cell RNA sequencing data. Genome Biol. 2015; 16: 278. doi: 10.1186/s13059-015-0844-5 [PubMed: 26653891]

69. Tran HTN, et al. A benchmark of batch-effect correction methods for single-cell RNA sequencing data. Genome Biol. 2020; 21: 12. doi: 10.1186/s13059-019-1850-9 [PubMed: 31948481]

70. Johnson WE, Li C, Rabinovic A. Adjusting batch effects in microarray expression data using empirical Bayes methods. Biostatistics. 2007; 8: 118–127. DOI: 10.1093/biostatistics/kxj037 [PubMed: 16632515]

Europe PMC Funders Author Manuscripts

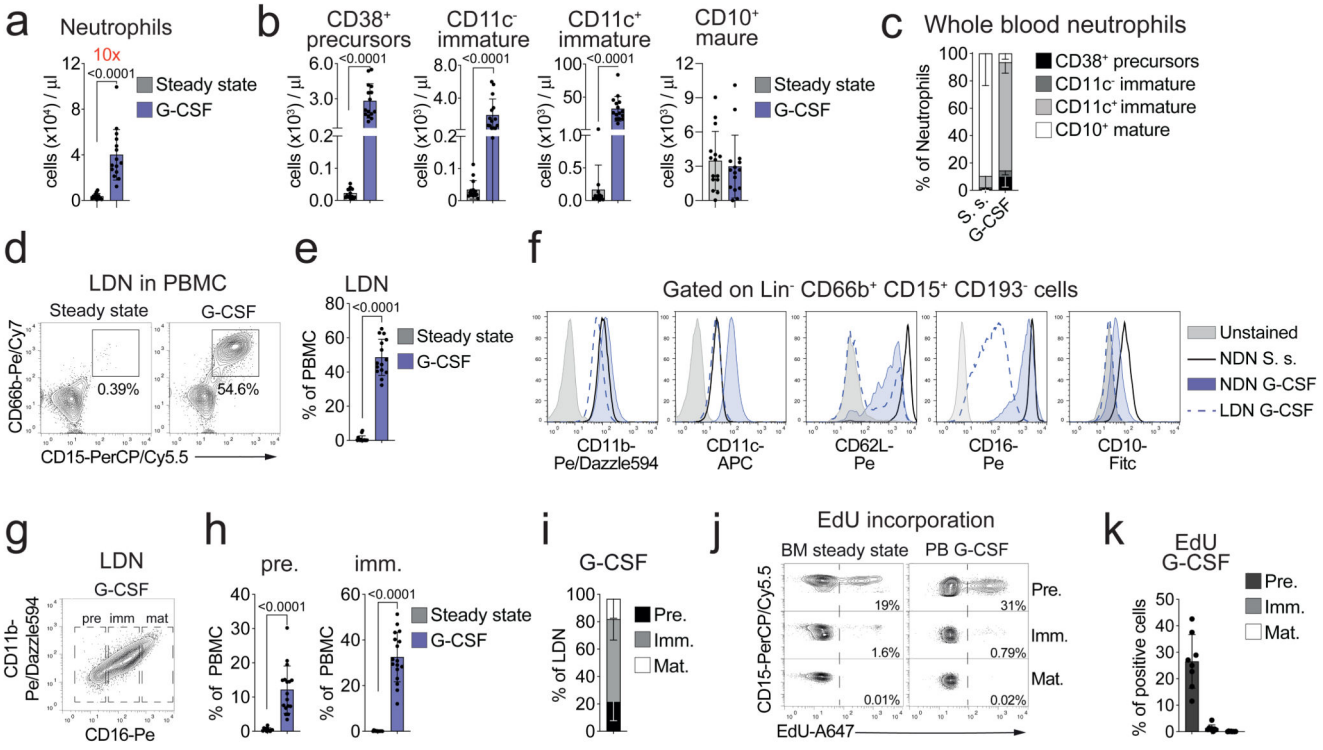

Fig. 1. Dynamics and phenotype of neutrophils elicited by G-CSF.

a. Absolute counts of neutrophils (gated as CD45$^+$ CD33$^+$/CD66b$^+$ SSC^{hi}) in whole PB of controls or G-CSF-treated donors (n=15). **b, c** Absolute counts (**b**) and percentage (**c**) of neutrophil subsets (gated as shown in Extended Data Fig. 1a) in whole PB of controls (n=15) or G-CSF-treated donors (n=15). **d, e.** Representative contour plots (**d**) or cumulative histogram plots (**e**) showing the frequencies of low-density neutrophils (LDNs) in the PBMC fraction of controls (n=16) and G-CSF-treated donors (n=15). **f**. Histogram plots showing representative expression levels of the indicated markers in normal density neutrophils (NDNs) from PB of controls (n>10) or G-CSF-treated donors and LDN of G-CSF-treated donors (n>12). **g.** Gating strategy used to identify neutrophil precursors (pre), immature (imm) and mature (mat) neutrophils within LDNs. **h, i.** Percentage of neutrophil precursors, immature and mature neutrophils within the PBMC fraction (**h**) or within LDNs (**i**) in controls (n=12) and G-CSF-treated donors (n=17). **j, k**. Representative contour plots (**j**) and cumulative histogram plots (**k**) showing percentages of EdU$^+$ cells within neutrophil precursors, immature and mature neutrophils in controls (n=3) or G-CSF-treated donors (n=8). Gating strategies for the indicated cell types are reported in Extended Data Fig. 1a-c and Supplementary Table 7. Bar plots represent data as mean ± SD. Numbers in red represent fold increases in the indicated conditions. Statistical analyses. **a**, **b**, **e**, and **h**: two-sided Mann-Whitney test.

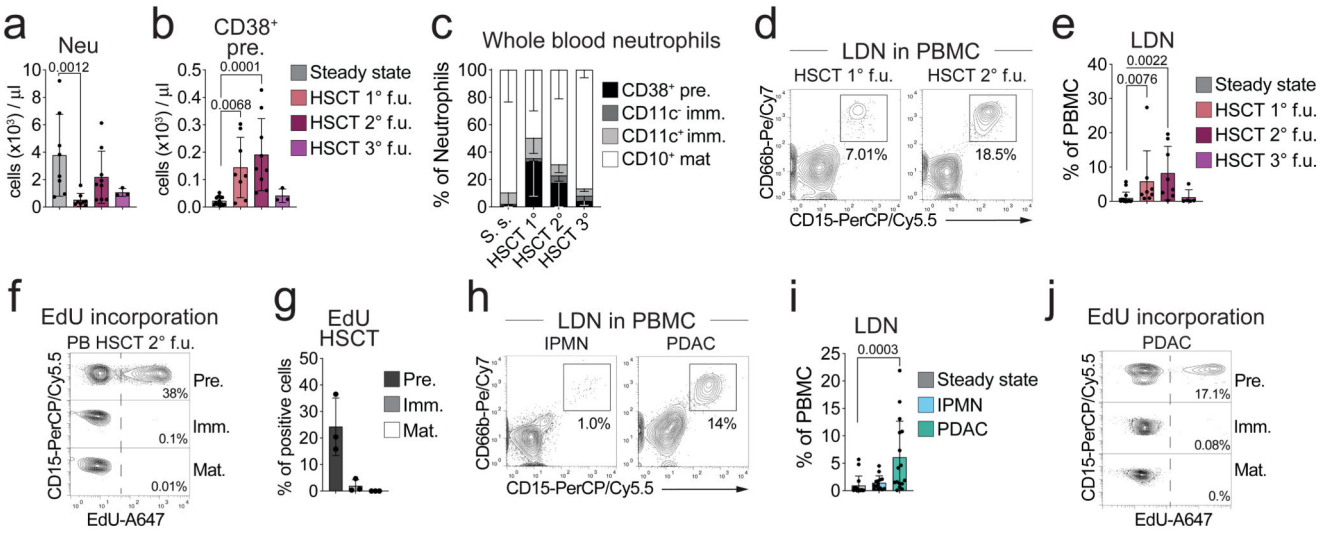

Fig. 2. Dynamics and phenotype of neutrophils during HSC-T or PDAC.

a. Absolute counts of neutrophils in whole PB of controls (n=8) or HSC-T patients (1° f.u. n=8, 2° f.u. n=9, 3° f.u. n=3). **b, c**. Absolute counts (**b**) and percentage (**c**) of neutrophil subsets (gated as shown in Extended Data Fig. 1a) in whole PB of controls (n=8) or HSC-T patients (1° f.u. n=7, 2° f.u. n=8, 3° f.u. n=3). **d, e**. Representative contour plots (**d**) or cumulative histogram plots (**e**) showing the frequencies of LDNs in the PBMC fraction of controls (n=16) and HSC-T patients (1° f.u. n=8, 2° f.u. n=8, 3° f.u. n=5). **f, g.** Representative contour plots (**f**) and cumulative histogram plots (**g**) showing percentages of EdU^+ cells within neutrophil precursors, immature and mature neutrophils in PB samples of HSC-T patients (2° f.u. n=3). **h, i.** Representative contour plots (**h**) or cumulative histogram plots (**i**) showing the frequencies of LDNs in the PBMC fraction of controls (n=16), IPMN (n=14), and PDAC patients (n=16). **j.** Representative contour plots showing percentages of EdU^+ cells within neutrophil precursors, immature and mature neutrophils in PB samples of PDAC patients. Gating strategies for the indicated cell types are reported in Extended Data Fig. 1a-c and Supplementary Table 7. Bar plots report data as mean ± SD. Statistical analyses. **a, b, e** and **i**: Kruskal-Wallis test plus two-sided Dunn's multiple comparison.

Europe PMC Funders Author Manuscripts

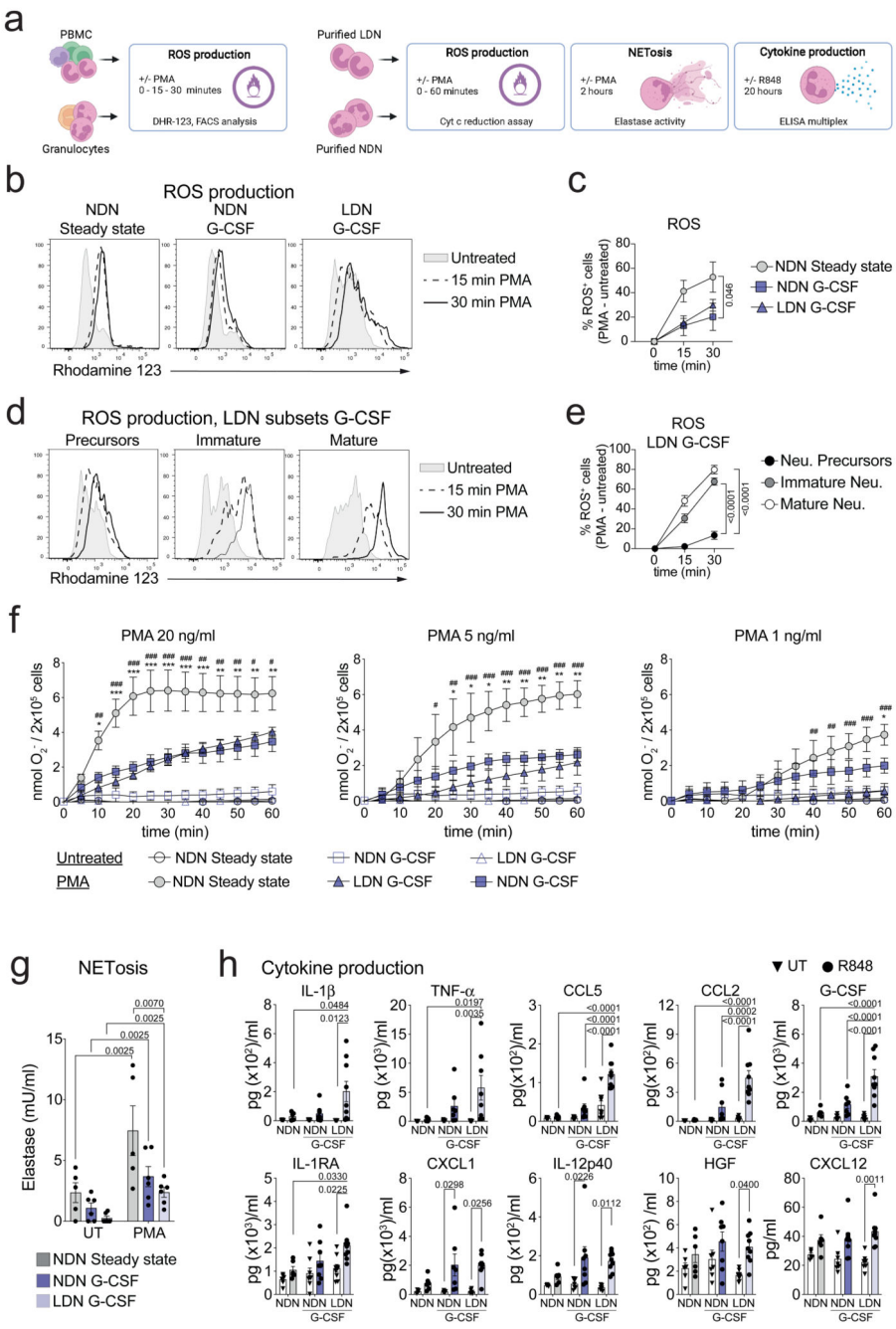

Fig. 3. Functional analysis of G-CSF-elicited neutrophils.

a. Schematic description of *ex vivo* experiments performed to evaluate ROS production, NETosis, and cytokine release by neutrophils. **b.** Representative histogram plots showing Rhodamine 123 signal in PMA-stimulated NDNs and LDNs from controls and G-CSF treated donors. **c.** Line plot showing percentage of ROS^+ cells in PMA-stimulated NDNs and LDNs from controls (n=2) and G-CSF treated donors (n=5). **d.** Representative histogram plots showing Rhodamine 123 signal in PMA-stimulated neutrophil precursors, immature, and mature neutrophils from G-CSF-treated donors. **e.** Line plot showing percentage of

Europe PMC Funders Author Manuscripts

Europe PMC Funders Author Manuscripts

ROS^+ cells in PMA-stimulated neutrophil precursors, immature, and mature neutrophils from G-CSF-treated donors (n=5). **f**. Line plots showing ROS levels in PMA-stimulated NDNs and LDNs from controls (n=3) or G-CSF-treated donors (n=3). **g**. Cumulative histogram plot showing PMA-induced NET release in NDNs and LDNs from controls (n=5) and G-CSF treated donors (n=6). **h**. Cumulative histogram plots showing the concentration of indicated cytokines released by R848-stimulated NDNs and LDNs from controls (n=6) or G-CSF-treated donors (n=8). Gating strategies for the indicated cell types are reported in Supplementary Table 7. Bar plots and line charts report data as mean ± SEM. Statistical analyses. **c, e, f, g** and **h**: Two-way ANOVA plus Tukey's multiple comparisons test. In panel **f** asterisks refer to the comparison between NDNs from controls versus G-CSF-treated donors; hashes refer to the comparison NDNs from controls versus LDNs from G-CSF-treated donors. * or # *p*-value < 0.05; ** or ## *p*-value < 0.01; *** or ### *p*-value < 0.001; **** or #### *p*-value < 0.0001; full p-values are reported in source data.

Europe PMC Funders Author Manuscripts

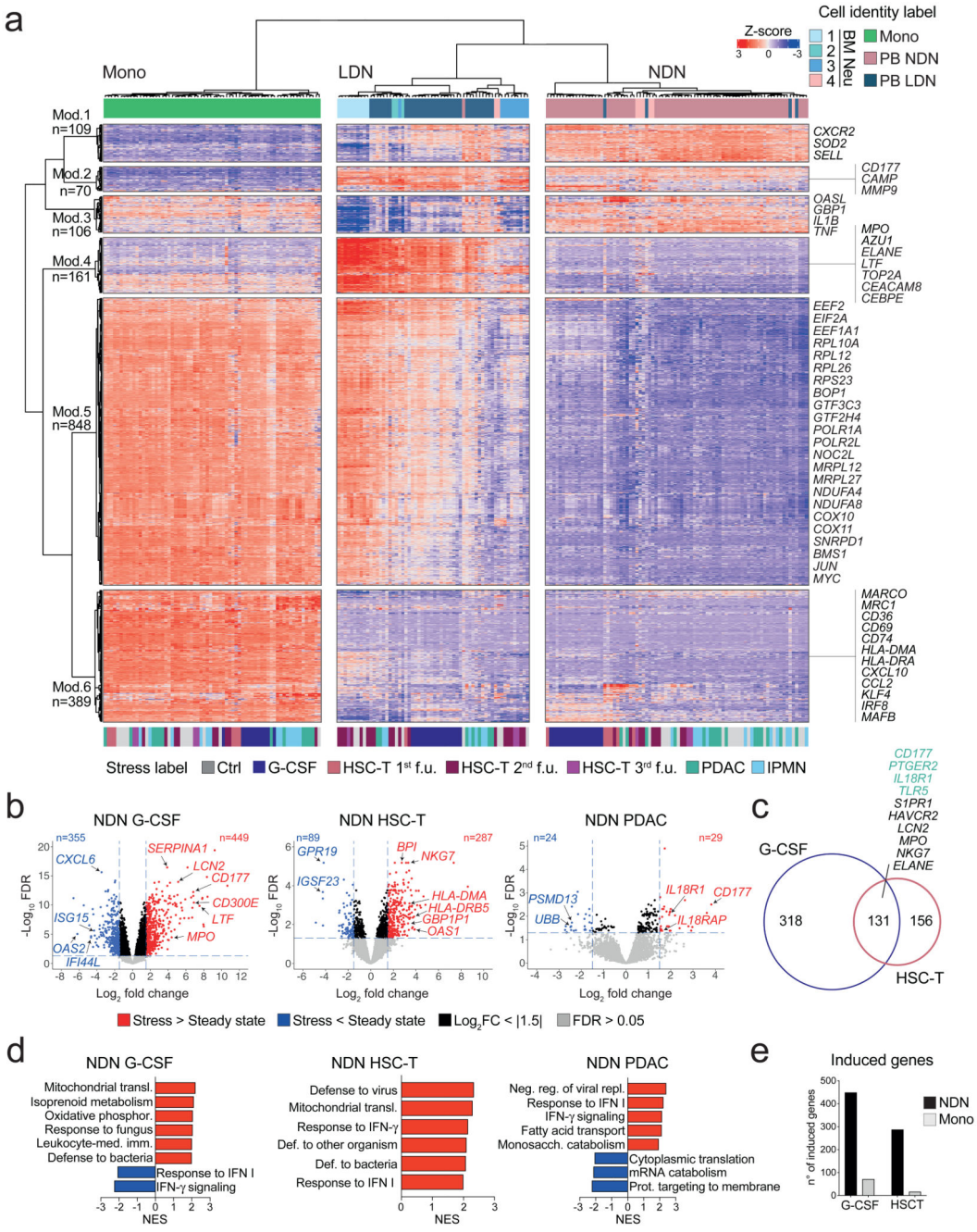

Fig. 4. Bulk RNA-Seq of neutrophils and monocytes upon G-CSF, HSC-T, IPMN or PDAC.

a. Heatmap showing normalized expression levels (Z-score) of variable genes (n=1,684, see Methods) in NDNs, LDNs and monocytes isolated from PB or BM of healthy controls (n=19), G-CSF-treated donors (n=17), HSC-T (n=8), PDAC (n=15) and IPMN (n=14) patients as well as of developing BM neutrophils from healthy donors (n=3) and HSCT patients (n=7). The row dendrogram represents hierarchical clustering of gene modules identified by k-means, and the column dendrogram represents hierarchical clustering of RNA-Seq samples. Legends and color bars at the top indicate sample identities by cell type

and at the bottom by experimental condition. Numbers on the row dendrogram represent the identity and size of each gene module, with representative transcripts shown on the right. Gating strategies for cell sorting are reported in Extended Data Fig.3a-f and Supplementary Table 7. See Supplementary Table 8 for the full list of samples (n=210). **b.** Volcano plots showing differentially expressed genes in NDNs from G-CSF-treated donors, HSC-T (1st and 2nd follow-up) or PDAC patients as compared to steady-state controls. The *x*- and y-axes indicate the expression fold change (log2) and the false discovery rate (FDR) (-$\log_{10}$) for each gene versus controls, respectively. Legends highlight up-regulated (red) or down-regulated (blue) transcripts, as well as genes not passing cut-off criteria for fold change (black) and FDR (grey) (see Methods). Selected representative genes are shown. **c**. Venn diagram showing the overlap between genes up-regulated in NDNs isolated form G-CSF treated donors or from HSC-T patients. Genes in green are also induced in NDNs isolated from PDAC patients. See Supplementary Table 13. **d.** Bar plots showing the normalized enrichment score (NES) of selected gene ontology (GO) categories enriched within genes up-regulated (red) or down-regulated (blue) in NDNs from the indicated experimental condition versus controls. **e**. Bar plot showing the number of genes induced ($\log_2$FC >1.5 and FDR < 0.05) in NDNs and monocytes isolated from G-CSF-treated donors or from HSC-T patients.

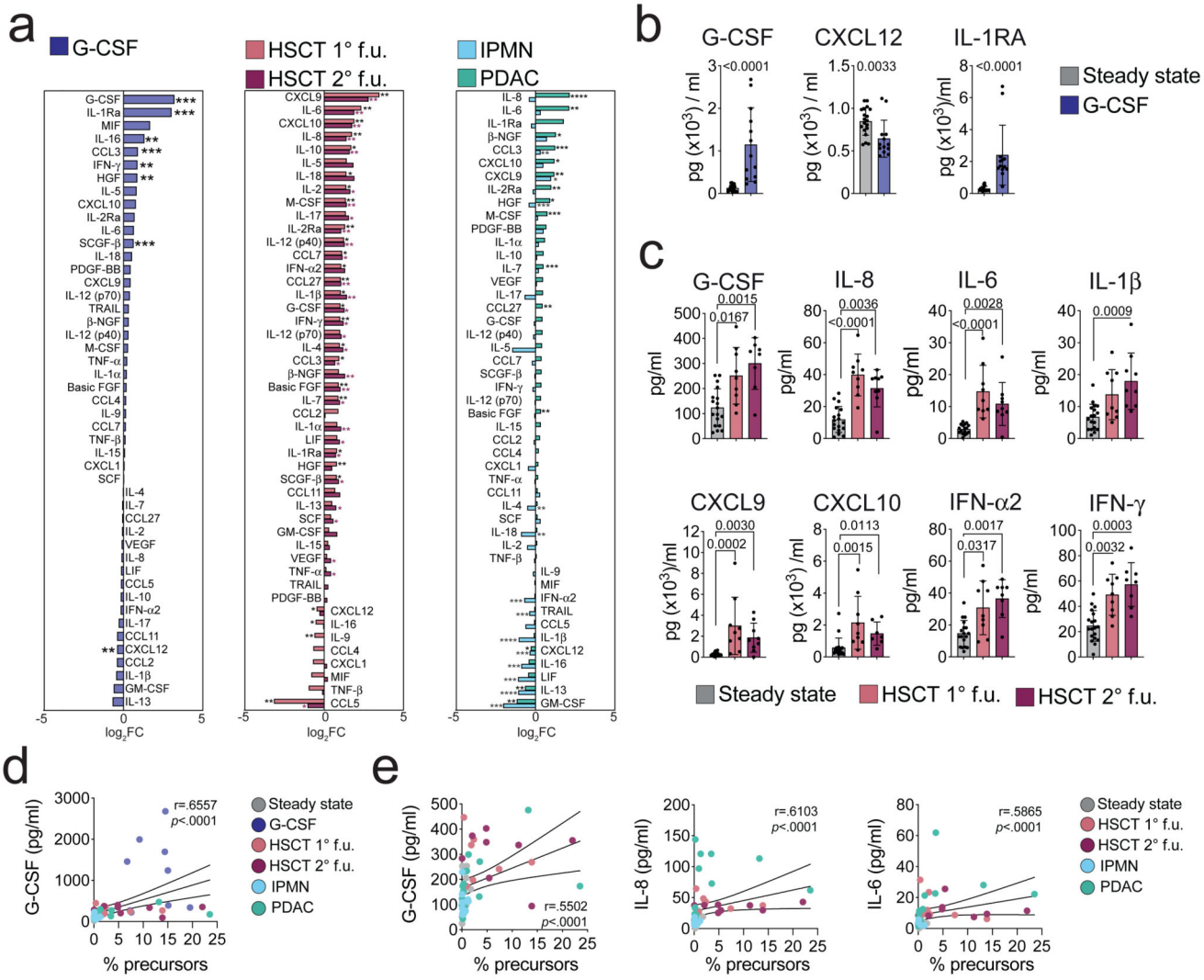

Fig. 5. Plasma factors underlying stress myelopoiesis upon G-CSF, HSC-T, IPMN or PDAC.

a. Bar plots showing the fold change of the mean concentration of the indicated factors in the plasma of G-CSF-treated donors, HSC-T, IPMN or PDAC patients as compared to controls (steady state n= 19; G-CSF n=13; HSCT 1° f.u. n=9; HSCT 2° f.u. n=9; IPMN n=15; PDAC n=18). **b, c.** Concentration of selected factors in the plasma of controls and G-CSF-treated donors (**b**) or controls and HSC-T patients at the indicated follow-ups (**c**) (steady state n=19; G-CSF n=13; HSCT 1° f.u. n=9; HSCT 2° f.u. n=9). **d, e**. Correlation between plasma concentrations of the indicated factors and frequencies of neutrophil precursors in the PMBC fraction, combining all samples together (**d**) or excluding (**e**) G-CSF-treated donors. Spearman's correlation and p-values are shown for each plot (steady state n= 14; G-CSF n=9; HSCT 1° f.u. n=7; HSCT 2° f.u. n=8; IPMN n=14; PDAC n=16). Cumulative bar plots report data as mean ± SD. Statistical analyses. **a**: Wilcoxon signed-rank test followed by FDR calculation with two-stage step-up method of Benjamini, Krieger and Yekutieli; **b**: two-sided Mann-Whitney test; **c**: Kruskal-Wallis test plus two-sided Dunn's multiple comparison; **d** and **e**: Spearman's correlation. **a**: **p*-value

< 0.05; ** *p*-value < 0.01; *** *p*-value < 0.001; **** *p*-value < 0.0001; full p-values are reported in source data.

Europe PMC Funders Author Manuscripts

This is an Adobe® Illustrator® File that was saved without PDF Content.
To Place or open this file in other applications, it should be re-saved from Adobe Illustrator with the "Create PDF Compatible File" option turned on. This option is in the Illustrator Native Format Options dialog box, which appears when saving an Adobe Illustrator file using the Save As command.

This is an Adobe® Illustrator® File that was saved without PDF Content.
To Place or open this file in other applications, it should be re-saved from Adobe Illustrator with the "Create PDF Compatible File" option turned on. This option is in the Illustrator Native Format Options dialog box, which appears when saving an Adobe Illustrator file using the Save As command.

This is an Adobe® Illustrator® File that was saved without PDF Content.
To Place or open this file in other applications, it should be re-saved from Adobe Illustrator with the "Create PDF Compatible File" option turned on. This option is in the Illustrator Native Format Options dialog box, which appears when saving an Adobe Illustrator file using the Save As command.

This is an Adobe® Illustrator® File that was saved without PDF Content.
To Place or open this file in other applications, it should be re-saved from Adobe Illustrator with the "Create PDF Compatible File" option turned on. This option is in the Illustrator Native Format Options dialog box, which appears when saving an Adobe Illustrator file using the Save As command.

This is an Adobe® Illustrator® File that was saved without PDF Content.
To Place or open this file in other applications, it should be re-saved from Adobe Illustrator with the "Create PDF Compatible File" option turned on. This option is in the Illustrator Native Format Options dialog box, which appears when saving an Adobe Illustrator file using the Save As command.

This is an Adobe® Illustrator® File that was saved without PDF Content.
To Place or open this file in other applications, it should be re-saved from Adobe Illustrator with the "Create PDF Compatible File" option turned on. This option is in the Illustrator Native Format Options dialog box, which appears when saving an Adobe Illustrator file using the Save As command.

This is an Adobe® Illustrator® File that was saved without PDF Content.
To Place or open this file in other applications, it should be re-saved from Adobe Illustrator with the "Create PDF Compatible File" option turned on. This option is in the Illustrator Native Format Options dialog box, which appears when saving an Adobe Illustrator file using the Save As command.

This is an Adobe® Illustrator® File that was saved without PDF Content.
To Place or open this file in other applications, it should be re-saved from Adobe Illustrator with the "Create PDF Compatible File" option turned on. This option is in the Illustrator Native Format Options dialog box, which appears when saving an Adobe Illustrator file using the Save As command.

Fig. 6. Single-cell RNA-Seq analysis of human neutrophils at steady-state and upon stress.

a. UMAP plot showing scRNA-Seq transcriptomes of 130,628 cells, sorted as CD15$^+$ neutrophils from whole PB or BM samples of healthy controls (PB n=2, BM n=2), G-CSF-treated donors (n=4), HSC-T (PB n=3, BM n=2) and PDAC (n=5) patients. Colors and numbers indicate clusters at resolution 1.5. Representative marker genes are shown for selected clusters. Groups of clusters corresponding to developing neutrophil subsets are indicated on the right. Pie charts report the frequency of PB or BM cells and of cells from controls, G-CSF-treated donors, HSC-T and PDAC patients. Clusters 25, 26 and 27 were

classified as contaminants. **b.** UMAP plots showing colored according to tissue of origin (PB/BM) and the stress condition. **c.** Heatmap showing expression of up to 50 marker genes for each scRNA-Seq cluster, with selected transcripts highlighted on the left or on the right. Color bars indicate cluster identities. Clusters of contaminants are not shown. **d.** Bar plots showing NES of selected GO categories enriched within combined marker genes of clusters 4 and 7 (corresponding to mature PB neutrophils from HSC-T patients at the 1st follow-up). **e, f.** Box plots showing the expression levels of combined marker genes of clusters 4 and 7 in neutrophil precursors, early immature, immature, and mature neutrophils from PB (**e**) or BM (**f**) samples from steady-state controls and HSC-T patients at the indicated follow-ups. Sample sizes are reported in Supplementary Table 27. FDR-adjusted p-values were calculated by two-sided Wilcoxon rank-sum test. Box plots represent the median, interquartile range (IQR), minimum (25th percentile, 1.5 × IQR) and maximum (75th percentile, 1.5 × IQR).

Europe PMC Funders Author Manuscripts

Europe PMC Funders Author Manuscripts

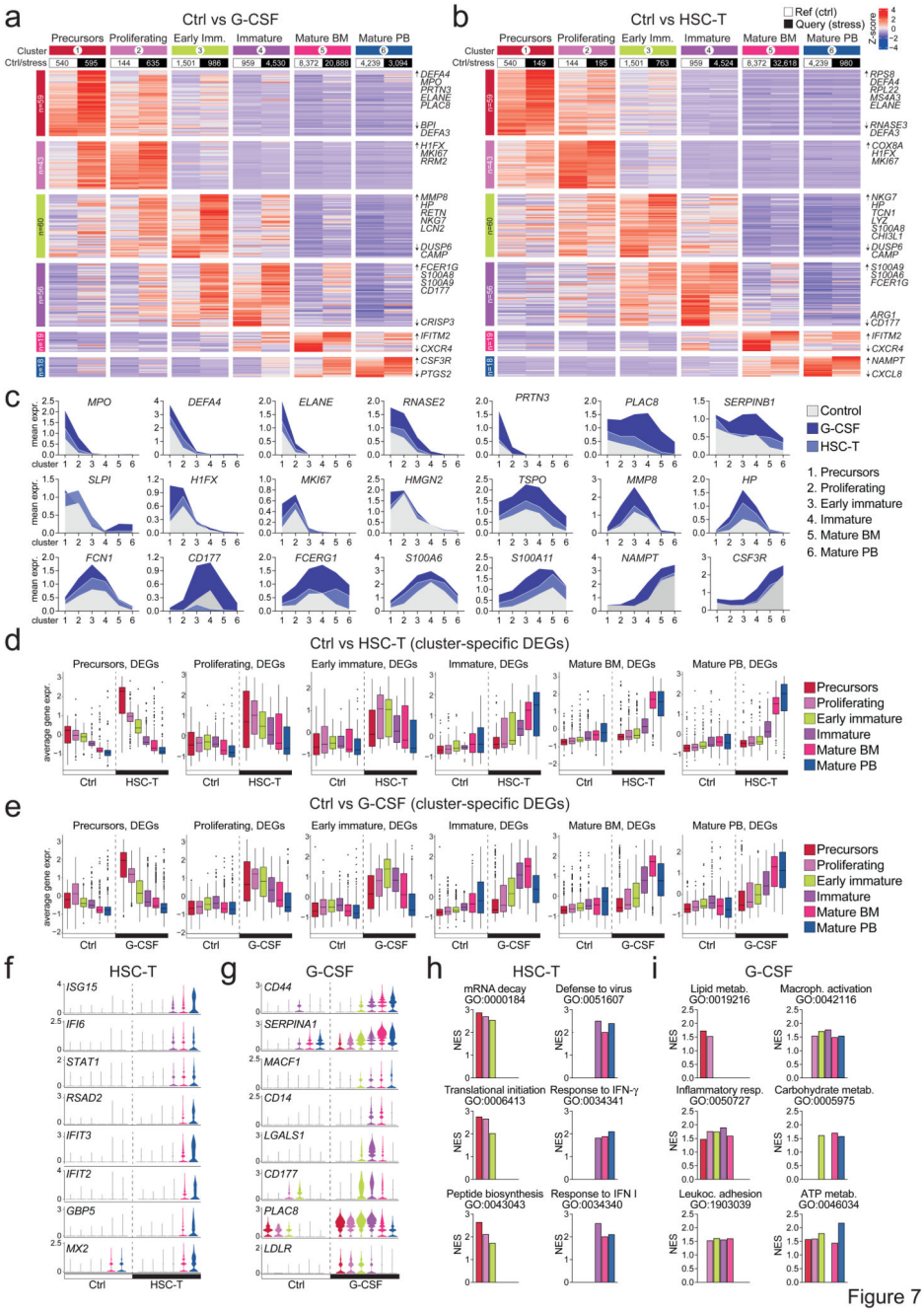

Figure 7

Fig. 7. Transcriptome reprogramming of human neutrophils upon stress.

a, b. Heatmaps showing standardized average expression (computed on normalized expression levels) of developmental marker genes identified by Cell Harmony and expressed in at least 20% of cells from reference datasets, for the indicated neutrophil subsets in controls (reference, white bars) and G-CSF-treated donors (**a**) or HSC-T patients (**b**) (query, black bars). The following samples were included in the Cell Harmony analysis: PB and BM for healthy controls; PB (all time points) and BM (day 30 and > 180 post-transplant) for HSC-T patients; PB from G-CSF-treated donors; PB from PDAC patients. Colored bars and

numbers represent stages of neutrophil development (1-precursors, 2-proliferating, 3-early immature, 4-immature, 5-mature BM, and 6-mature PB) after alignment of scRNA-Seq data with Cell Harmony (see Methods). The number of cells from reference and query datasets for each cluster is shown at the top, the number of developmental marker genes for each cluster is shown on the left. Selected representative genes are highlighted on the right. **c.** Filled area plots showing mean expression in scRNA-Seq data of selected developmental marker genes in neutrophil subsets from controls (grey), G-CSF-treated donors (dark blue) or HSC-T patients (light blue). Numbers on the x-axis indicate the stages of neutrophil development identified by Cell Harmony. **d, e**. Box plots showing standardized average expression of genes up-regulated (see Methods) in the indicated neutrophil subsets from HSC-T patients (**d**) or G-CSF-treated donors (**e**) versus controls. Each plot refers to induced genes in query versus reference scRNA-Seq datasets for neutrophils at each stage of development defined by Cell Harmony. Box plots represent the median, interquartile range (IQR), minimum (25th percentile, 1.5 × IQR) and maximum (75th percentile, 1.5 × IQR). Sample size corresponds to the number of cells indicated in the heatmaps (**a, b**). **f, g.** Violin plots showing normalized expression levels of selected genes induced in mature neutrophils from HSC-T patients (**f**) or G-CSF-treated donors (**g**) as compared to controls. Colors represent stages of neutrophil development defined by Cell Harmony. **h, i.** Bar plots showing NES of selected GO categories enriched within genes expressed at higher levels in neutrophil subsets from HSC-T patients (**h**) or G-CSF-treated donors (**i**) as compared to controls. Colors represent stages of neutrophil development defined by Cell Harmony.

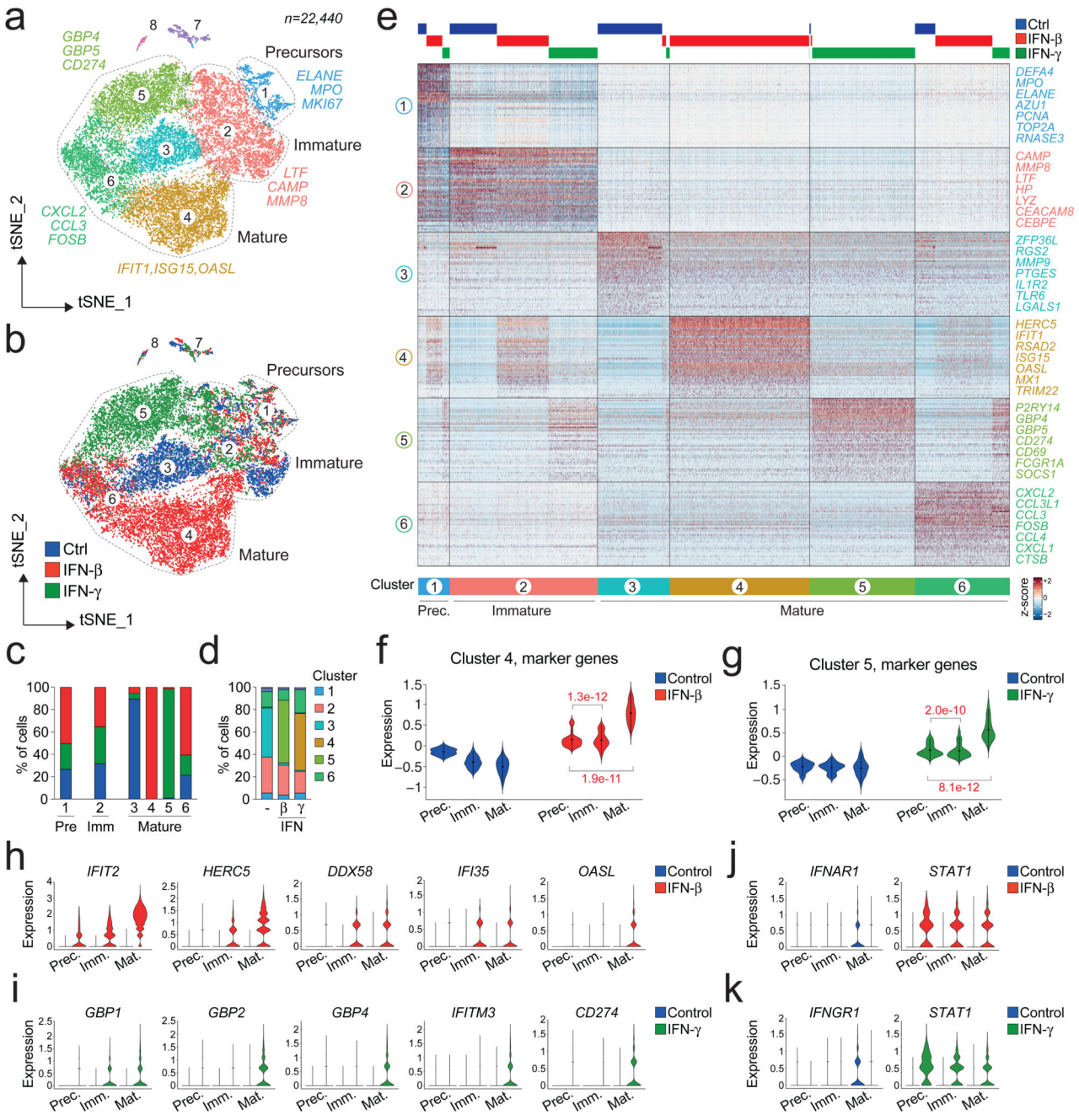

Fig. 8. Maturation stage-dependent transcriptome dynamics in neutrophils stimulated with IFNs.

a, b. t-distributed stochastic neighbor embedding (tSNE) plots showing scRNA-Seq transcriptomes of 22,240 cells, isolated as neutrophils (see Methods and Extended Data Fig. 10a-d) from CB samples and stimulated *ex vivo* with IFN-β or IFN-γ for 4 hours. Colors and numbers represent clusters at resolution 0.3 (**a**), or the type of treatment (**b**). Representative marker genes are shown for selected clusters. Groups of clusters corresponding to developing neutrophil subsets (precursors, immature and mature) are indicated. Clusters 7 and 8 were classified as contaminants. **c.** Stacked bar plots showing

the fraction of cells corresponding to control (blue), IFN-β (red) or IFN-γ (green) treatment conditions for the indicated scRNA-Seq clusters. **d.** Stacked bar plots showing the fraction of cells belonging to scRNA-Seq clusters for the indicated culture condition. **e.** Heatmap showing normalized expression (Z-score) of up to 50 marker genes for each scRNA-Seq cluster, with selected transcripts highlighted on the right. Cluster identities and corresponding classifications as precursors, immature or mature neutrophils is shown by color bars at the bottom. Color bars at the top indicate cells corresponding to control (blue), IFN-β (red) or IFN-γ (green) treatments. **f, g.** Violin plots showing mean standardized expression of top 25 marker genes of cluster 4 (mature neutrophils, IFN-β-treated) (**f**) or cluster 5 (mature neutrophils, IFN-γ-treated) (**g**) in cells corresponding to neutrophil precursors, immature and mature neutrophils from controls or the indicated stimulation conditions; p-values were calculated by two-sided Wilcoxon rank-sum test. **h, i.** Violin plots showing normalized expression of selected genes induced by IFN-β (**h**) or IFN-γ (**i**) in cells corresponding to neutrophil precursors, immature and mature neutrophils from controls or the indicated stimulation conditions. **j, k.** Violin plots showing normalized expression of the genes encoding for IFN receptors and signaling molecule STAT1 in cells corresponding to neutrophil precursors, immature and mature neutrophils from controls or the indicated stimulation conditions.